CSIRO PUBLISHING

Review

www.publish.csiro.au/journals/ajc

Aust. J. Chem. **2003**, *56*, 981–1000

Meditation on an Engraving of Fricke and Klein (The Modular Group and Geometrical Chemistry)

Stephen T. Hyde,[A,B] *Ann-Kristin Larsson*,[A] *Tiziana Di Matteo*,[A] *Stuart Ramsden*[A] *and Vanessa Robins*[A]

[A] Department of Applied Mathematics, Research School of Physical Science, Australian National University, Canberra 0200, Australia.

[B] Author to whom correspondence should be addressed (e-mail: stephen.hyde@anu.edu.au).

A non-technical account of the links between two-dimensional (2D) hyperbolic and three-dimensional (3D) euclidean symmetric patterns is presented, with a number of examples from both spaces. A simple working hypothesis is used throughout the survey: simple, highly symmetric patterns traced in hyperbolic space lead to chemically relevant structures in euclidean space. The prime examples in the former space are derived from Felix Klein's engraving of the modular group structure within the hyperbolic plane; these include various tilings, networks and trees. Disc packings are also derived. The euclidean examples are relevant to condensed atomic and molecular materials in solid-state chemistry and soft-matter structural science. They include extended nets of relevance to covalent frameworks, simple (lattice) sphere packings, and interpenetrating extended frameworks (related to novel coordination polymers). Limited discussion of the projection process from 2D hyperbolic to 3D euclidean space via mapping onto triply periodic minimal surfaces is presented.

Manuscript received: 29 July 2003.
Final version: 4 August 2003.

Introduction

The mysteries of higher mathematics are often neglected by the chemist, who manages to create increasingly complex atomic and molecular-scale self-assemblies despite that neglect. Nature's solutions to mutual spatial arrangements of atoms or molecules, from metallo-organic ligands in modern metal-coordination polymers or lyotropic liquid crystals to materials as banal as silica, are often more clever and elegant than theory can concoct.

We recall a conversation with a senior Australian colloid chemist at an international conference a decade ago. 'What has topology to do with colloidal assemblies?' one of us was asked after delivering a lecture at an international conference on colloid science that sought to link topology and molecular self-assembly. A belated, oblique response is this paper, which seeks connections between non-euclidean geometry, group theory, and the structures of atomic and molecular materials. ('... Probably about as much as hyperbolic non-euclidean geometry.')

The paper deals with symmetric packings, networks, and spatial partitions. It is a preliminary survey of the tight connections that exist between symmetric patterns in different spaces. We do not intend to offer a systematic exploration of non-euclidean and euclidean patterns here. The prime purpose of this paper is to argue a simple, though not widely appreciated, thesis: Chemists recognize the centrality of symmetric patterns in understanding condensed atomic, molecular, and colloidal aggregates. To that end, various approaches to generation and systematic cataloguing of symmetric patterns have been developed. However, so far, no universal toolkit exists, that spans the array of forms found in condensed atomic, molecular, polymeric, and colloidal materials. One promising generic approach is the exploration of symmetric tilings and packings in two-dimensional hyperbolic space and subsequent mapping into conventional three-dimensional euclidean space. That approach has the following attractive features.

- Highly symmetric hyperbolic tilings (whose symmetries are commensurate with euclidean symmetries) produce symmetric structures, affording a natural 'filter' to deduce chemically useful structures.
- Many euclidean structures can result from a single hyperbolic one.
- A broad spectrum of structural objects result readily. For examples
  - Projections of tilings with finite-sided tiles produce 3D translationally periodic nets, including arrays of 2D and 3D nets.
  - Projections of trees (infinite sided tiles) produce multiple interpenetrating nets.

The case is demonstrated by a number of constructions derived from simple hyperbolic patterns. Those constructions are related to the solid and semi-solid state and are relevant

 10.1071/CH03191 0004-9425/03/100981

to atomic crystals, covalent frameworks, coordination polymers, and liquid crystals formed by larger molecules, such as amphiphiles or molten block copolymers.

The paper is organized in two parts. Some familiarity with non-euclidean geometry is needed to comprehend the wealth of form available in hyperbolic space. Accordingly, the first part consists of ruminations on hyperbolic geometry, inspired by a famous image of Felix Klein (written up by his collaborator Robert Fricke), found in a masterwork of 19th century mathematics: *Vorlesungen über die Theorie der elliptischen Modulfunktionen* (figure 35 of volume 1).[1] To the student of non-euclidean geometry, the image reveals many of the riches of the symmetries of 2D hyperbolic geometry. To the group and number theorist, it is equally rich. For the purposes of this paper, we view Klein's image through the lens of geometry. Klein's modular group tiling is a springboard for the later constructions. We first explore the concept of symmetries in hyperbolic space and its relation to conventional euclidean 2D symmetries, with the help of 'orbifold' theory, developed recently. We then extract features of the Klein image, with particular emphasis on symmetric tilings with polygonal faces and symmetric packings of infinite 'trees', devoid of closed faces. En route, a number of observations about the nature and peculiarities of hyperbolic space are noted, in part for their intrinsic interest, in part for their relevance to 3D symmetric patterns. In particular, the character of ideal polygons (peculiar to hyperbolic space) and their bewildering variety of tiling possibilities is discussed. In addition, very low density disc packings are explored for their possible relevance to low density (and therefore highly porous) framework materials in 3D euclidean space. The first part concludes by transposing the most interesting features of Klein's image to a slightly different symmetry setting, in order to admit projection to 3D euclidean space.

The second section explores features of possible forms in 3D euclidean space that hint at a wealth of structural complexity. The forms are related to hyperbolic patterns described in the preceding section, by a specific projection process. Projections used here invoke only the simplest projection 'substrates', the 3D crystalline minimal surfaces of cubic symmetry. Details of the projection are ignored as they require some analysis of differential geometry

Hyde, Larsson, Di Matteo, Ramsden, and Robins

Stephen Hyde has been in the Department of Applied Mathematics of the Australian National University (ANU) since 1986, after gaining his Ph.D. from Monash University, Melbourne, and an extended period with Sten Andersson in Lund. He is interested in understanding structure and morphology in nature in terms of geometry and topology.

Ann-Kristin Larsson was born in Gothenburg, Sweden, in 1963. She completed her Ph.D. at the University of Lund in solid state chemistry/crystallography in 1995 then undertook a two-year postdoc at the Research School of Chemistry, ANU. Between 1997 and 2002 she was a research associate at the University of Stockholm, and is now back at the ANU, this time in Applied Mathematics. Her main scientific interest is combining crystallographic techniques such as X-ray and electron diffraction and electron microscopy to describe materials in a new and useful manner.

Tiziana Di Matteo graduated from the Physics Department of Salerno University in Italy in 1994, where she also obtained her Ph.D. in physics in 1999. She is currently a Queen Elizabeth Fellow at the Department of Applied Mathematics, ANU. Since 1999, the major focus of her research has been the study of networks and the application of physics methods to financial markets. She is studying complex systems using techniques of statistical physics, non-linear dynamical analyses, and numerical computational methods.

Stuart Ramsden is a visualization programmer at the ANU Supercomputer Facility and consultant at the ANU Department of Applied Mathematics. His interests include non-euclidean geometry, computational topology, algorithmic tiling theory, and crystallography, as well as procedural modelling and animation.

Vanessa Robins received her Ph.D. in 2000 for work on computational topology supervised by Jim Meiss and Liz Bradley at the University of Colorado, Boulder. She is currently a postdoctoral scholar at ANU. Her research interests cover various applications of geometry and topology in the physical sciences.

and group theory. (Indeed, we are still in the process of developing those analytical techniques.) Our purpose here is to reveal by example the richness of this approach. We consider here three- and four-coordinated tilings to generate extended three-coordinated and four-coordinated crystalline frameworks. We also explore in some detail the projections to 3D euclidean space of hyperbolic 'forests', consisting of close-packed trees. These examples prove to be particularly interesting, allowing for multiple interpenetrating extended frameworks, as well as laminations and interweavings of extended (often warped) planar frameworks (or 'nets'). The nature of interpenetration is discussed briefly, as the approach affords useful insights into classification and control of interpenetrating nets. Lastly, we show that these interpenetrating nets can be used to derive novel surface partitions of space that combine features of better-known partitions, such as honeycombs and sponges, in novel ways.

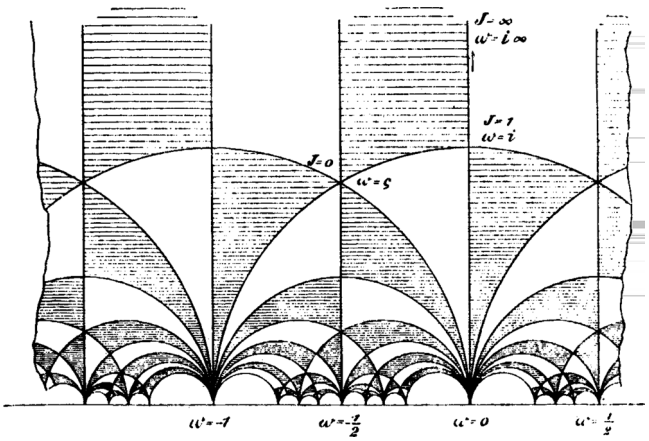

Fig. 1. Hand-carved engraving of the upper half-plane model of 2D hyperbolic space of the symmetries of the modular group. From Fricke and Klein's encyclopedic tome *Theorie der automorphen Funktionen*.[1]

Hyperbolic Geometry, Tilings, and Disc Packings in the Modular Group

The origins of Klein's image are impressive, and confirm the profound connection between geometry and number theory. Two versions of the image are available, and the first apparently appears in the papers of Gauss, though Fricke and Klein have a wonderfully clear image in their tome, *Theorie der automorphen Funktionen* (Fig. 1). It is a tiling of the upper half (complex) plane by triangles made up of semi-circular arcs, with vertex angles $\pi/3$, $\pi/2$, and 0. Tiles are alternately shaded light and dark. The tiling defines symmetries of the 'modular group', and the map conserves the angular structure of those symmetries. (The uppermost tiles appear to be four-sided. Formally, the two vertical sides are considered to meet at a single point—infinity. That notion implies that these tiles too are triangles.)

These transformations define symmetries of Klein's multiply periodic automorphic functions (similar to the usual singly-periodic circular trigonometric functions). In addition to the apparent translational periodicity, the modular group is a *non-euclidean kaleidoscope*, by analogy with toy (euclidean) kaleidoscopes. The group is replete with *mirror reflections*.

To appreciate the subtlety of those symmetries, it is convenient to map the upper half-plane model of Gauss onto the unit disc, by means of a standard transformation that is conformal (that is, it displays all angles with their true values in hyperbolic space). That operation gives the pattern so carefully engraved in the book of Fricke and Klein (Fig. 2). Notice that indeed, the smallest tiles are triangles with vertex angles of $\pi/2$, $\pi/3$, and 0, and the edges remain circular arcs of variable radius. In this image, the zero-angle vertices are located around the perimeter of the unit disc, with all edges meeting the perimeter at $\pi/2$. The picture can be read as an image of a non-euclidean 2D space, the

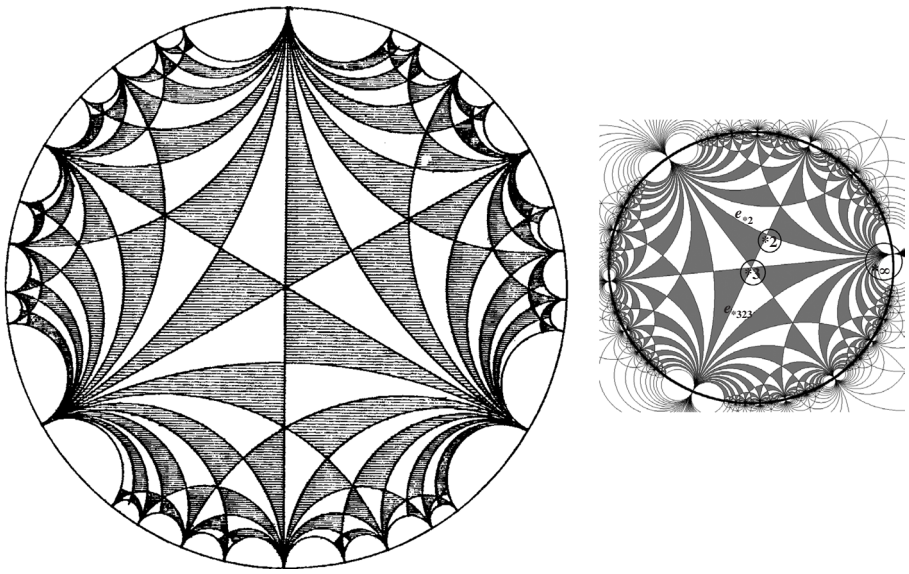

Fig. 2. Fricke and Klein's engraving of the modular group, drawn within the Poincaré disc model of 2D hyperbolic space. Inset: Our digital redraft of their figure, labelled to reveal distinct vertices of types *2 and *3 and edges e_{*2} and e_{*323}.

hyperbolic plane ($\mathcal{H}^2$). This is Poincaré's disc model of that space, in which the analogues of euclidean lines (hyperbolic geodesics) are described by circular arcs. The boundary of the disc, the unit circle, defines points in $\mathcal{H}^2$ that are infinitely distant from its origin. Circular arcs that intersect the unit circle orthogonally correspond to geodesics of $\mathcal{H}^2$. Poincaré's model is astonishingly compact, with massive shrinkage of $\mathcal{H}^2$ to squeeze it into the unit disc of the euclidean plane ($\mathcal{E}^2$), $\mathcal{D}^2$. That shrinkage is again conformal, so that the angles between arcs are exactly those in the hyperbolic space $\mathcal{H}^2$. The arrangement of geodesics in Figure 2 is that of mirror reflection lines of the modular group.

The symmetry group of that pattern is thus kaleidoscopic. The entire space $\mathcal{H}^2$ can be covered without gaps or overlaps by a triplet of reflection geodesics, intersecting at $\pi/2$, $\pi/3$, and 0 (just as a conventional toy kaleidoscope is formed by mirrors meeting at angles commensurate with flat space; for example three mirrors subtending angles of $\pi/3$ with each other). We label the symmetry of the modular group by its *Conway orbifold symbol*,[2] *23∞. (Conway and Schäfli notation are outlined more fully in the Appendix.) Orbifold symbols provide a compact label for all 2D symmetry groups. The symbol describes the symmetry operations within a fundamental domain of the group, consisting of sites of rotational symmetry, labelled by digits (i for an i-fold rotation point) followed by mirror paths, denoted by the string '*$abc\ldots$', describing mirrors intersecting at angles of π/a, π/b, $\pi/c\ldots$. (Glide reflections and translations are also possible, but not needed here.) We label vertices of the *23∞ pattern of Figure 2 according to their site symmetries—Those within the interior are either *2 or *3 vertices, common to four and six edges respectively; edges are of two types, those passing through *2 vertices only, and those passing through a single *2 and a pair of *3 vertices, labelled as e_{*2} and e_{*323} respectively (Fig. 2 inset).

The possibility of zero-angle vertices in hyperbolic polygons has no precedent in euclidean geometry. The zero-angle edges are parallel to each other and 'meet at infinity'. (Indeed, the zero angle vertices in Figure 2 all lie on the perimeter of $\mathcal{D}^2$.) An infinite number of geodesics meet at these boundary points, so that these points are common to an infinite number of *23∞ triangles! We note that all ideal polygons $\{n_\infty\}$ with the same number of sides (n) are congruent.

Hyperbolic Tilings

The richness of $\mathcal{H}^2$ symmetries compared with the euclidean plane is overwhelming. Indeed, there are an infinite number of hyperbolic orbifolds, including an infinite number of kaleidoscopic examples.

A concrete geometric expression of symmetries can be found in *tilings*. A tile is a shape (or shapes) that tessellates the space without gaps or overlaps. We consider here only the simplest *regular* tilings, containing a *single* tile whose symmetry is as high as possible, consistent with the related symmetry group. Examples of such tilings in $\mathcal{E}^2$ are well known: they are the square, triangular, or hexagonal tilings, and subdivisions or gluings thereof. We denote a tiling by its Schläfli symbol, $\{n,z\}$, for an n-sided tile, with z neighbours sharing each vertex (see also the Appendix). We adopt the following convention. *Regular* tilings, with identical vertices, edges, and faces, carry the symbol $\{n,z\}$, while less-symmetric irregular examples are denoted (n,z). Consider first the symmetry of regular tilings. Each tile, $\{n\}$, has a centre of n-fold rotational symmetry, where n mirrors meet, giving site symmetry *n. In addition, vertices have symmetry *z and edges *2 at their mid-points, generating a *2zn kaleidoscope. In general then, $\{n,z\}$ tilings have kaleidoscopic symmetries, with Conway orbifold symbol *2zn, and the tessellation is produced by the orbit of a vertex at the *z site under the action of the mirrors. (Notable exceptions to this behaviour are discussed below.) Thus, decoration of the *236 orbifold gives the 2D euclidean 'wallpaper' tiling of regular triangles (Fig. 3*a*). Similarly, the *23∞ kaleidoscope of Fricke and Klein defines a regular tiling of $\mathcal{H}^2$, $\{3,\infty\}$, by ideal triangles, $\{3_\infty\}$ (an ideal triangle with vertices at ∞); Fig. 3*b*.

Trees

Closer inspection of Fricke and Klein's engraving reveals a sequence of ideal polygons, $\{z_\infty\}$, for all integers $z > 2$, formed by fusing $z-2$ ideal triangular faces (Fig. 4*a*). The tessellations, $\{3,\infty\}$ and $\{4,\infty\}$—regular tilings of $\mathcal{H}^2$—are thus also contained as subgraphs of Fricke and Klein's image (Fig. 4*b*)!

These exotic tilings lead to even less familiar *duals*. The dual is obtained by swapping vertices and faces; the dual of $\{n,z\}$ is $\{z,n\}$. We construct the dual tilings by replacing each face by a single vertex at the in-circle centre of that face, and extend edges between all faces sharing a common edge in the original tiling. Duals $\{\infty,z\}$ of the $\{z,\infty\}$ tilings of ideal polygons described in the previous paragraph contain infinite-sided regular polygons, with vertex angles of $2\pi/z$. The edges of these tilings are *regular* z*-coordinated trees*, also generated from the hyperbolic kaleidoscopic groups *2$z\infty$. (An example for the $z=3$ case is shown in Fig. 9*a*). Indeed, vertices of trees (∞,z) are coincident with vertices in Figure 2 for each integer $z > 2$. (Recall parentheses '()' indicate that the tilings are irregular and contain inequivalent faces, edges, and vertices.) Note, however, that regular trees $\{\infty,z\}$ cannot be traced in the image of Fricke and Klein for $z > 3$ as the highest-order symmetry sites are *3, and higher polygons $\{z\}$ require *z sites.

One further subtlety surrounding tilings by ideal polygons remains hidden within Fricke and Klein's image. Distinct symmetries can be found for the regular $\{z,\infty\}$ tilings and their duals, in addition to the regular kaleidoscopic groups *2$z\infty$. For example, mirrors can be successively removed, leading to lower symmetries. This possibility too is a unique feature of $\mathcal{H}^2$; as discussed above, regular tilings of $\mathcal{E}^2$ are necessarily kaleidoscopic. For example, *2$\infty\infty$, 3*$\infty\infty$, and $32^\infty (= 3222\ldots)$ orbifolds can be decorated to produce $\{3,\infty\}$ tilings (Figs. 5 and 6). The reason for a variety of symmetries can be traced to the peculiar geometry of ideal polygons. As all edges are parallel, an individual tile is free to slide relative to its neighbours along any boundary edge without displacing other tiles. All these $\{z,\infty\}$ patterns can

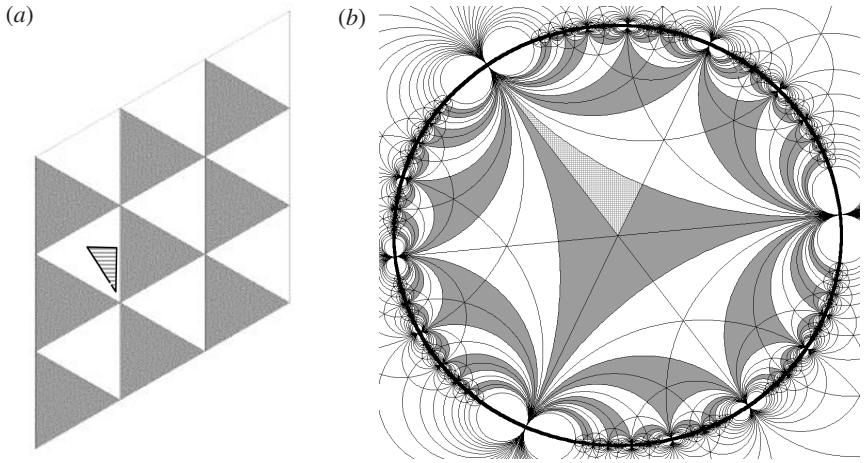

Fig. 3. (*a*) Regular {3,6} tiling of the euclidean plane $\mathcal{E}^2$. (Alternate tiles are shaded for clarity only.) A region corresponding to a single fundamental domain of the *236 kaleidoscopic orbifold, bounded by three mirror lines, is hatched. (*b*) Poincaré disc model of a regular {3,∞} tiling of $\mathcal{H}^2$ with identical ideal triangles. A region corresponding to a single fundamental domain of the *23∞ kaleidoscopic orbifold, bounded by three mirror lines, is hatched. (Curves beyond the bold unit disc are not relevant to the tiling.)

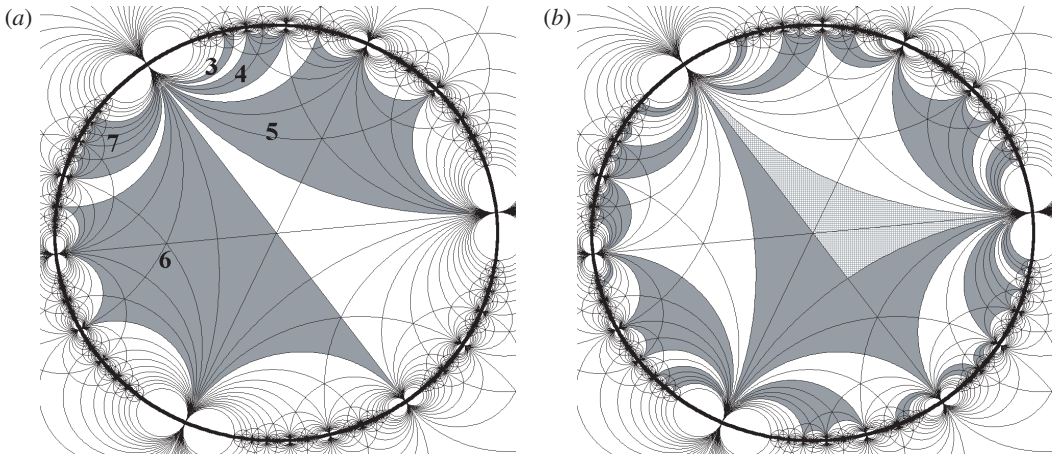

Fig. 4. (*a*) Ideal polygons within Klein's pattern. Highlighted clockwise from top left: triangle, quadrilateral, pentagon, hexagon, and septagon. (*b*) Regular {4,∞} tiling of $\mathcal{H}^2$, with a single *2∞∞ hatched orbifold.

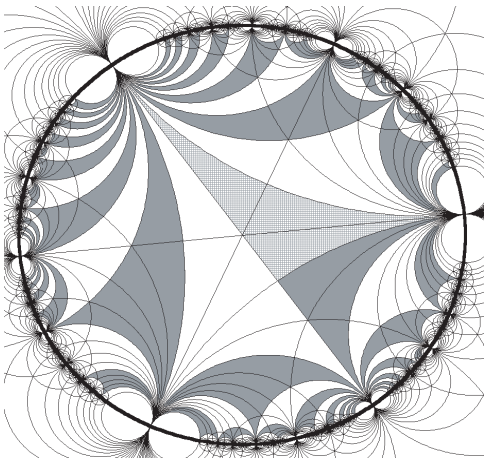

Fig. 5. Regular tiling {3,∞} of $\mathcal{H}^2$ derived from Figure 2, built with ideal triangles, $\{3_\infty\}$ displaying orbifold symmetry *2∞∞. A single fundamental domain (half a single tile) is hatched.

be symmetrized to regain the most symmetric $*2z\infty$ pattern, through displacement of tiles along either of the edges e_{*2} or e_{*323}. However the duals of these patterns differ markedly from each other, revealing yet a further novel feature of $\mathcal{H}^2$ geometry.

Low Density Disc Packings

We now consider patterns formed by locating hyperbolic discs at vertices of Klein's tiling. Hyperbolic disc packings are analogous to circle and sphere packings in euclidean space, and the well-known concepts of packing density and stability can be applied to disc packings in $\mathcal{H}^2$ without difficulty. Packing density describeds the filling fraction (by area) of the discs within $\mathcal{H}^2$. The area of a hyperbolic disc of radius r is

$$2\pi\cosh(r-1) = 2\pi\left(\frac{r^2}{2!} + \frac{r^4}{4!} + \cdots\right) \qquad (1)$$

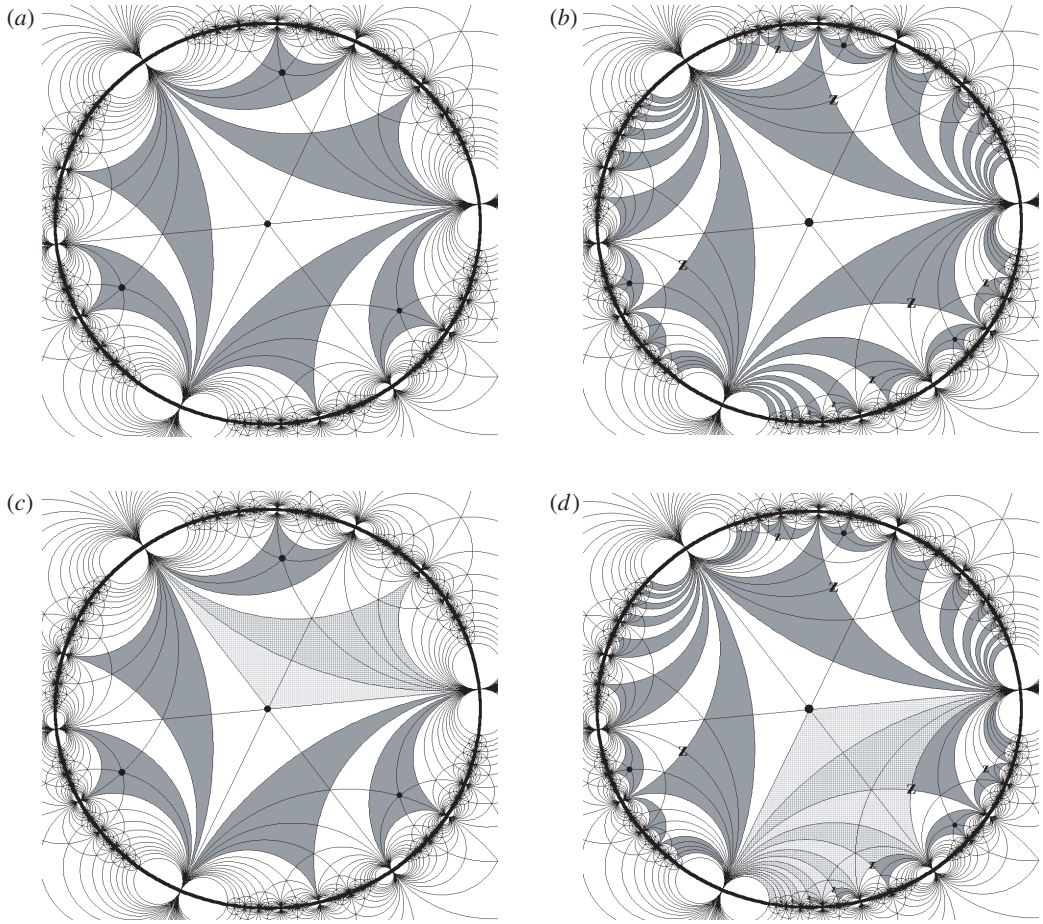

Fig. 6. Irregular tilings (3,∞) of $\mathcal{H}^2$ derived from Figure 2, all containing regular ideal triangles. (*a*) 3*∞∞ (three-fold sites coincident with vertices of Fig. 2 dotted); (*b*) 32^∞ or 3222... (three-fold sites dotted, two-fold sites marked with 'z'); (*c*) and (*d*) show fundamental domains of the relevant orbifolds for (*a*) and (*b*) respectively (cross-hatched). Notice that the fundamental domain of the patterns (*b*) and (*d*) is infinitely large, containing a single 3-fold and an endless number of distinct 2-fold sites!

Hyperbolic space allows huge latitude in forming symmetric disc packings, from very low density patterns to very dense ones. Since the tilings—regardless of symmetry—are (z,∞), all dual tilings are trees, (∞,z), also denoted here $T(l, z)$ (or $T\{l, z\}$ for regular examples). Irregular trees contain symmetrically inequivalent $\{z_\infty\}$ faces in the lower symmetry $\{z,\infty\}$ patterns. For example, the 32^∞ pattern contains distinct $\{3_\infty\}$ faces: those with 3-fold rotational symmetries at their centres, and those with 2-fold sites on an edge. The dual (∞,z) tree thus contains distinct vertices, some with equal edge angles ($2\pi/z$) and some without (Fig. 6). Further, the edge lengths of the trees depend on their symmetry. The edge lengths l of regular trees (with symmetry *2$z\infty$) can be calculated from the formula relating edges l with angles α, β, γ:

$$\operatorname{arcosh}(l) = \frac{\cos(\alpha)\cos(\beta) + \cos(\gamma)}{\sin(\alpha)\sin(\beta)} \qquad (2)$$

The edge length of *2$z\infty$ trees $T\{l_c, z\}$ is thus (see also Fig. 9*a*)

$$l_c(i) = 2\operatorname{arcosh}\left(\operatorname{cosec}\frac{\pi}{2}\right) \qquad (3)$$

twice the in-circle radius of the $\{z\}$ polygon (compare Equation (*1*)). We can place a disc of radius $l_c/2$ at each tree vertex, forming a z-coordinated disc packing in $\mathcal{H}^2$ (see Fig. 7*a* for $z = 3$).

These are very low density ('rare') packings, whose fractional area covering of $\mathcal{H}^2$ (or packing density) is

$$\frac{4}{z-2}\sinh^2\left[\operatorname{arcosh}\left(\operatorname{cosec}\frac{\pi}{i}\right)\right] \qquad (4)$$

or 0.30940 and 0.41421 for 3- and 4-coordinated packings, respectively. That result follows from Equations (*1*) and (*2*).

Still rarer packings can be generated by the following process. Decorate each z-coordinated disc centred on vertices of the *2$z\infty$ tree by z smaller discs, arranged *rigidly* in the original disc so that each smaller disc is in contact with one other such disc and shares a single boundary point with the original disc (Fig. 7*b*). These decorated packings are now *all* 3-coordinated, with packing densities

$$\frac{4z}{z-2}\sinh^2\left(\frac{r}{2}\right) \qquad (5)$$

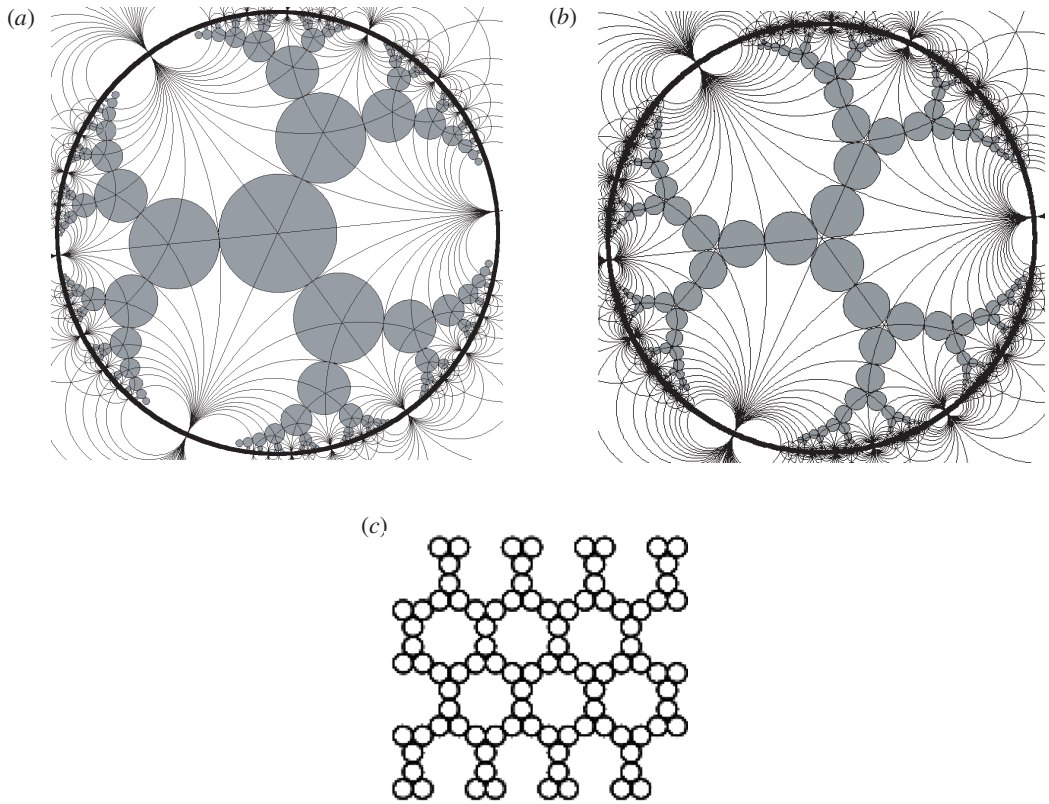

Fig. 7. Disc packings in (*a*) and (*b*) $\mathcal{H}^2$ and (*c*) $\mathcal{E}^2$. (*a*) Results from locating discs at *3 sites of Figure 2. (*b*) Results from 'decorating' each disc with three smaller nested discs. These packings exhibit very low densities ('rare'), and (*b*) is the natural hyperbolic analogue of the rarest euclidean 2D disc packing, shown in (*c*).

where r is the disc radius, equal to

$$\operatorname{artanh}\frac{\sqrt{\operatorname{cosec}^2(\pi/z)-1}}{2\operatorname{cosec}(\pi/z)} \qquad (6)$$

giving densities of 0.19677 and 0.27618 for rare packings formed by decoration of the 3- and 4-coordinated packings, respectively. These packings have a natural counterpart in 2D euclidean space, generated by decoration of the regular {6,3} tiling. The resulting packing is conjectured to be the rarest *rigid* disc packings in $\mathcal{E}^2$, of density $(7\sqrt{3}-12)\pi \approx 0.3907$ (Fig. 7*c*).[3] (A 'rigid' packing is locally stable; it cannot be perturbed without first swelling the entire array, thereby decreasing the packing density.)

The discs in the original undecorated rare packings are arranged in horocycles of $\mathcal{H}^2$ (euclidean circles of infinite radius). 'Peripheral' discs, located infinitely distant from the origin (tangentially grazing the boundary of the Poincaré disc), just touch, so that continuous loops can be traversed along the discs, from the origin to infinity and back again (Fig. 7*a*). Any shrinkage of the tree edges below l_c will result in crossings of tree edges. Söderberg has called such trees 'critical trees',[4] characterized by the critical edge length $l_c(z)$ (Equation (*3*)) for regular trees. We note that the rare z-coordinated packings shown in Figure 7 are not rigid. Discs can be displaced relative to each other without lowering the density since the common tangents to neighbouring discs lie on the edges of polygons, amenable to displacement relative to each other as described above. That displacement operation generates new disc packings—also not rigid. Alternatively, these can be generated by replacing all z_∞-gons by discs of radius a in irregular trees. Such arrangements are clearly realizable, as z_∞-gons tile $\mathcal{H}^2$ without gaps or overlaps. Notice, however, that in these irregular cases, discs are no longer z-coordinated so that the packings are not locally or globally dense; rather they are loose, and able to rattle against each other. Examples for $z = 3$ are shown in Figure 8.

The rattles can be removed, and the packing rendered rigid, by expanding the discs until they jam against each other. Thus, edges belonging to these irregular (∞,z) trees are *longer* than those of the $*2z\infty$ regular trees, $\{\infty,z\}$, demonstrating the relative rarity (in the sense of low density) of the $*2z\infty$ packings. This inverse correlation between symmetry and density (*high* symmetry inducing *low* density) is a notable one, encountered often in euclidean spaces also.

Forests

Yet another interesting class of patterns lies hidden within the engraving of Fricke and Klein: 'forests' of multiple trees. Consider first a countable sequence of regular trees, $\{\infty,3\}$, generated by connecting the neighbouring, next-nearest neighbouring, ... *3 points in Figure 2, as illustrated in Figure 9*a*. Denote the sequence of three-coordinated regular trees derived by this construction $T(l_i,3)$, where l_i denotes the edge length between connected i-th neighbouring *6 vertices. The first and last members of the family, $T(l_1,3)$ and

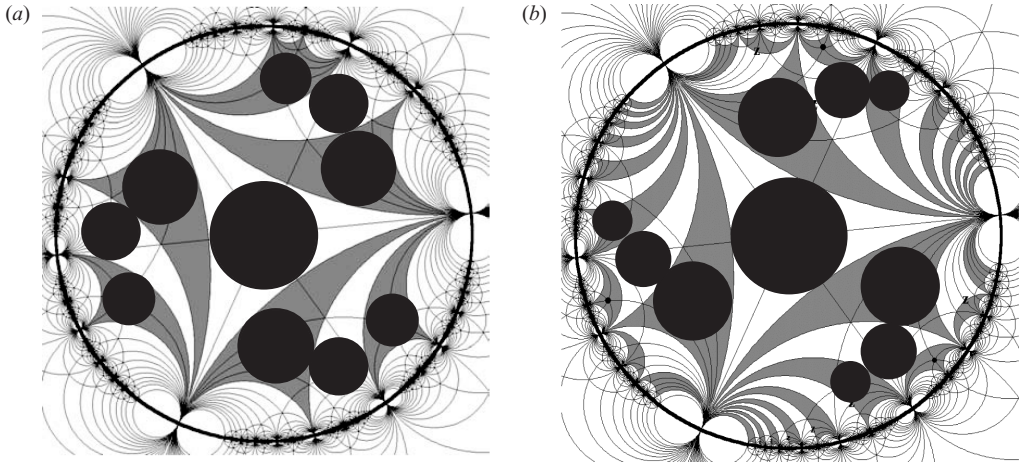

Fig. 8. Sketches of unstable disc packings formed by incircles of tiles of the (*a*) 3*∞∞ and (*b*) 32^{∞} patterns of Figure 5. In contrast to those in Figure 7, these packings are not rigid.

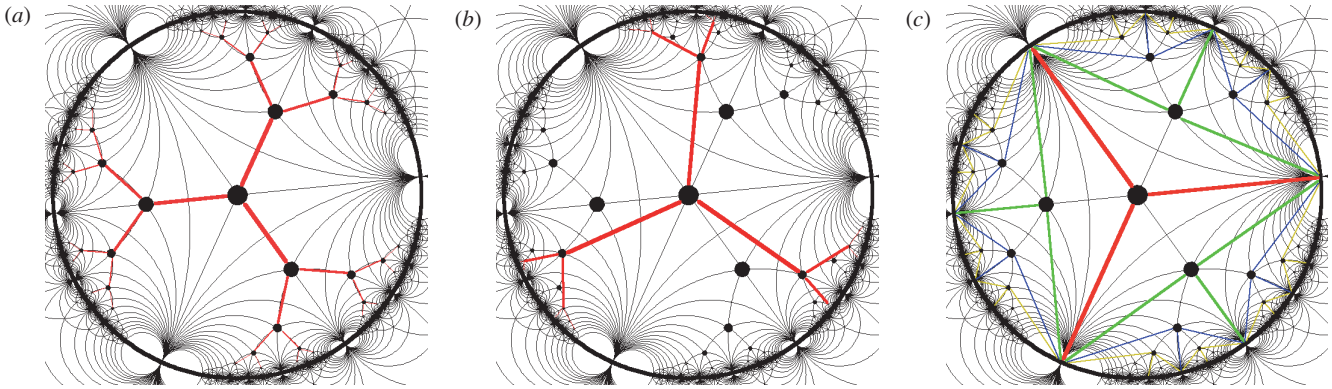

Fig. 9. Three members of the sequence of three-coordinated trees (red) with successively longer edges, superimposed on Klein's pattern (black). All tree vertices are (dotted) *3 sites. (*a*) A single regular 'critical' tree, with edge length $l_c(3)$ (Equation (*3*)) formed by joining nearest *3 neighbours, (*b*) next-nearest neighbouring *3 vertices of Klein's pattern, and (*c*) a number of close-packed 'star'-trees (with a single vertex per tree, and three edges joining next–next- . . . -neighbouring vertices), forming a regular forest. Successive trees are coloured red, green, blue, and yellow. Trees in (*b*) are irregular, while those in (*a*) and (*c*) are regular and their (geodesic) edges are contained in Klein's figure (although our sketch has non-geodesic edges).

$T(l_\infty, 3)$ are sub-graphs of the edges in the original engraving (while intermediate members are not, compare Fig. 9*b*).

Indeed, an infinite number of densely packed $T(l_\infty, 3)$ trees—a regular, dense forest with orbifold symmetry *23∞—can be traced in Fricke and Klein's engraving. Neighbouring 'trees' (actually star-like, containing only one vertex) in this dense forest are separated by geodesics e_{*2} (Figs. 2 and 9*c*) that reflect one tree into its neighbour. The geodesics e_{*2} coincide with the regular $\{3,\infty\}$ tiling introduced above (Fig. 3*b*). Recall that the symmetry of the $\{z,\infty\}$ patterns (Fig. 5) can be altered by sliding ideal polygonal tiles along their edges. In the same manner, the symmetry of the regular forest $T(l_\infty, 3)$ can be adjusted by relative displacement of neighbouring trees along the edges e_{*2}. That process allows the distance between neighbouring vertices (in adjacent trees) to lie in the interval [arcosh(5/3),∞), where the lower bound is found in the *23∞ forest of Figure 9*c* and larger values can be realized in forests of rotational symmetry 2323. For reasons described in the next section, we choose a displacement of arcosh(3). That case gives a 'coincident site lattice', with partial overlap of forest vertices with those of another group, *246, a supergroup of 2323.

Just as a countable family of trees can be found in the Fricke and Klein image, a family of forests, consisting of densely packed trees, $T\{\text{arcosh}(3),3\}$, $T\{\text{arcosh}(5),3\}, \ldots$ can be formed from successive vertices in the *246 tiling.[5] The tree vertices of all members of this family are identical; distinct members are formed by choosing different edges linking those vertices. Note that all these forests consist of 3-coordinated trees.

The most symmetric[6] example is that with the shortest edges, $T\{\text{arcosh}(3),3\}$ and orbifold symmetry *2223. Dense forests of z-coordinated trees can be formed in $\mathcal{H}^2$ with symmetry *222z; these examples contain vertices at the *z sites and tree edges along the e_{*z2z} edges of the hyperbolic kaleidoscope (generalizing the notation for edges introduced above). We can therefore construct dense forests with 3- *and* 4-coordinated trees commensurate with *246, since *2223

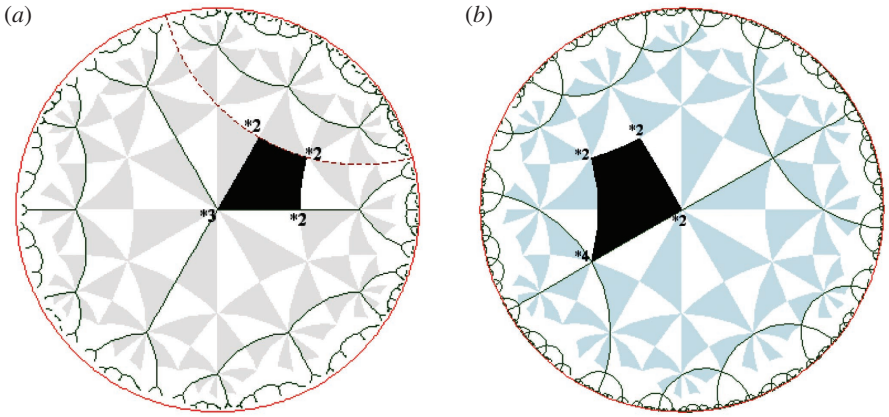

Fig. 10. 'Forests' of close-packed trees generated from a kaleidoscopic tiling of $\mathcal{H}^2$ by *246 domains (alternate tiles are shaded). (*a*) A *2223 forest with 3-coordinated trees, showing a single separating geodesic (linking adjacent *2 sites), with a fundamental domain highlighted in black. (*b*) A *2224 forest, containing 4-coordinated trees.

and *2224 are subgroups (orders 2 and 3 respectively) of *246. These forests contain trees of type $T\{\text{arcosh}(3),3\}$ and $T\{\text{arcosh}(5),4\}$ (Figs 10*a* and 10*b*, taken from ref. [5]).

Dense Disc Packings

The *24(6) tiling can be generalized to a *24($2z$) tiling; each integer $z \geq 3$ admits a one-parameter (λ) family of forests, consisting of densely packed z-coordinated regular trees, $T(\lambda, z)$. Discs can be centred at vertices of the z-coordinated forests, the vertices of regular $\{4,2z\}$ tilings, forming $2z$-coordinated dense, rigid packings (Fig. 11, $z = 3$). In contrast to the z-coordinated rare disc packings formed by placing discs on tree vertices, these $2z$-coordinated packings are dense, with packing fractions

$$\frac{4}{z-2}\sinh^2\left(\frac{r_z}{2}\right) \tag{7}$$

where r_z is the disc radius, equal to

$$\text{arcosh}\frac{\sqrt{1+\cos^2(\pi/2z)}}{\sin(\pi/2z)} \tag{8}$$

giving space-filling fractions of 0.82843 and 0.84776 for $z = 3$ and 4 respectively.

Still denser rigid disc packings are formed by inserting 4-coordinated (B) discs in the interstices of the dense $2z$-coordinated packings, centred at the vertices of a regular $\{2z,4\}$ tiling (Fig. 12*a*). The resulting binary rigid packing, with $4z$-coordinated (A) discs and 4-coordinated (B) discs, has stoichiometry A_2B_z and packing fraction

$$\frac{2z+4}{z-2}\sinh^2\left(\frac{\lambda_z}{2}\right) \tag{9}$$

where λ_z is the radius of the smaller interstitial (B) discs:

$$\lambda_z = \frac{1}{2}\text{arcosh}\left(\cot\frac{\pi}{z}\right) \tag{10}$$

These packings are very dense. Filling fractions for the A_2B_3 and AB_2 patterns ($z = 3$ and 4 respectively) are 0.9343 and 0.94110.[†]

The disc radii can be adjusted to give mixed $2z$ and 4-coordinated patterns with *equal* radii (R_z) for both A and B discs (Fig. 12*b*). The coordination of A discs is now $2z$ while that of B discs remains unchanged ($z = 4$). These packings have space-filling fractions of

$$\frac{2(2+z)}{z-2}\sinh^2\left(\frac{R_z}{2}\right) \tag{11}$$

where

$$R_z = \frac{1}{2}\text{arcosh}\left(\cot\frac{\pi}{2z}\right) \tag{12}$$

that is, filling fractions of 0.84385 and 0.91969 for $z = 3$ and 4 arrays (A_2B_3 and AB_2) respectively. Equalization of A and B disc radii to form non-overlapping, A_2B_z disc *24($2z$) symmetry packings is only possible for $z = 3$ and 4. (For $z > 4$ the B spheres are forced to overlap.)

Ribbons and Decorated Trees

A final structure of interest can be discerned in the image of Fricke and Klein—its dual. This 3-coordinated tiling is a fascinating pattern that we call a ribbon-decorated tree, with each vertex of the critical 3-coordinated *23∞ tree, $T(l_c(3), 3)$ decorated by a regular hexagon, $\{6\}$, and three half-squares, with all vertex angles equal to right angles (Fig. 13).

We can transpose this decoration process to form ribbon-decorated forests, commensurate with the *246 tiling. A number of geometries can be selected; we constrain the pattern to produce (4) and (6) polygons. Consider first that the forest with the shortest tree edges commensurate with *246, $T(\text{arcosh}(3),3)$ (Fig. 10*a*), giving the image of Figure 14.

Consider first the case where the polygons are regular. The vertex angles (α and β) are approximately 0.436π and

[†]The limit case for divergent z has no counterpart in euclidean space. Its packing fraction is 0.9610, exceeding that of the $2z$-coordinated packing of equivalent discs, 0.9003. Yet both packings have effective stoichiometry B (the former has stoichiometry A_2B_∞, or B) and the geometry of the B lattice is identical in both packings!

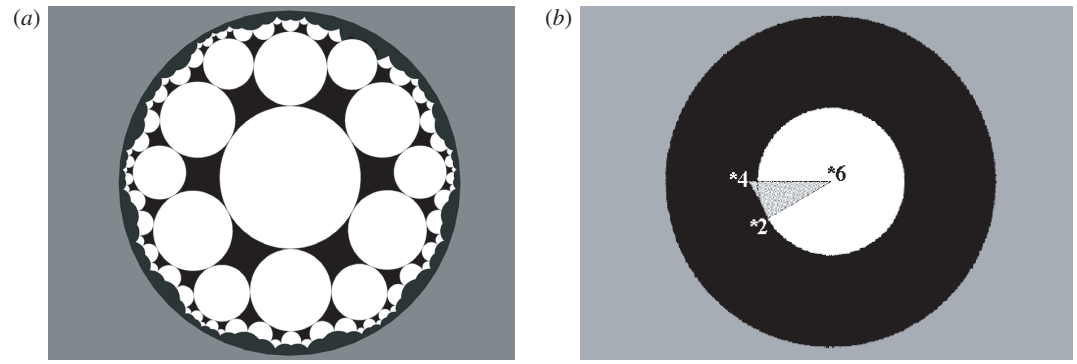

Fig. 11. (*a*) A dense, rigid, four-coordinated disc packing formed by locating discs on *6 vertices of the *246 pattern in $\mathcal{H}^2$. (*b*) Poincaré disc (entire $\mathcal{H}^2$) shown in black, overlaid with a single *246 domain (hatched triangle) and a central disc (white). The disc sector within the hatched domain generates the disc packing of (*a*) under the kaleidoscopic action of the *246 orbifold, namely reflections in edges of the hatched triangle.

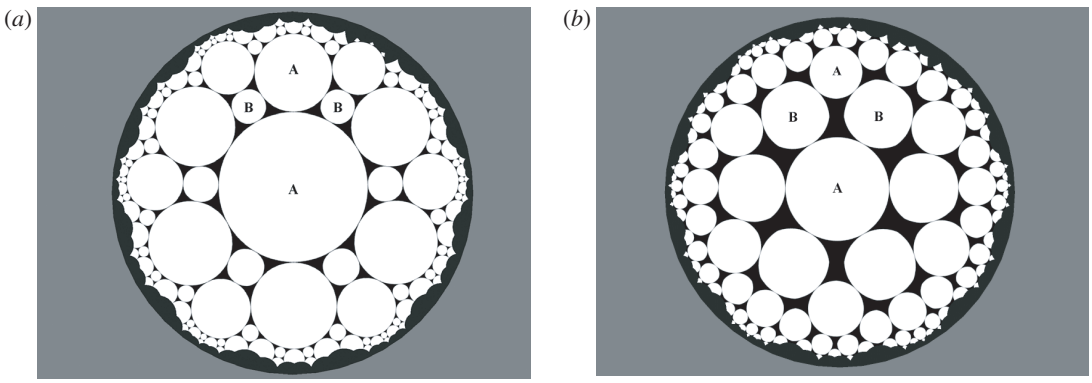

Fig. 12. Dense, rigid, binary (A_2B_3) 4- and 12-coordinated disc packing formed by locating discs on *6 vertices and *4 sites of the *246 pattern in $\mathcal{H}^2$. (*a*) Packing of Figure 11*a* ('A' discs) with extra interstitial B discs, tangential to the discs in Figure 11. (*b*) Disc packings with centres at the same locations as those in (*a*), formed by shrinking A discs and growing B discs to give congruent A and B discs.

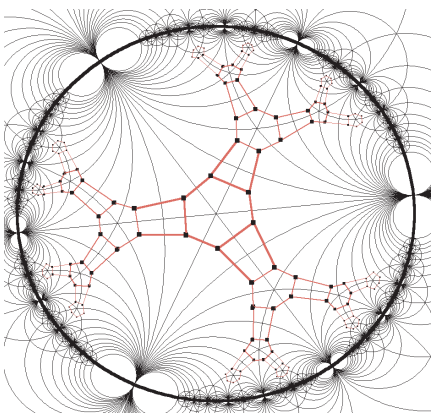

Fig. 13. Klein's pattern (dark) and its dual (red), generated by placing a dual vertex in every tile of the original pattern (incomplete sketch). The dual is a ribbon-decorated three-coordinated tree.

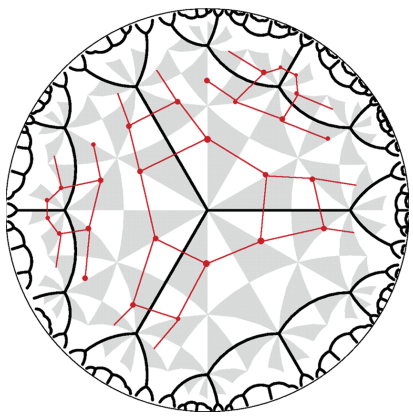

Fig. 14. Decoration of vertices of regular 3-coordinated trees commensurate with *246 symmetry (fundamental domains of *246 are alternately shaded triangles). The resulting pattern is a forest of ribbon-decorated trees. Each decorated tree is topologically identical to the dual of Figure 13.

0.564π for the {4} and {6} faces, respectively, and the shortest distance between edges of adjacent trees are about 0.368 times longer than the {6} and {4} edges. The regular {6} polygons can be grown at the expense of the (4)'s, until there is *just* enough space to accommodate regular {6} right-angled polygons, with edge length arcosh(2) (and no bridging (4) polygons, $s = 0$). This pattern is a regular net on $\mathcal{H}^2$, with identical vertices common to four {6} faces (6.6.6.6).

This process of decorating trees with ribbons can be generalized to arbitrary *$2z\infty$ trees, $T(l_c(i), i)$ (compare Equation (*3*)). For general values of z, the ribbon decoration then contains polygons ($2z$) and (4). For example, ribbon-decorated 4-coordinated trees, packed into a forest, consisting of {8} and {4} polygons, can be constructed.

From Hyperbolic to Euclidean Space

The motivation for this detailed exploration of 2D patterns in hyperbolic space lies in its relevance to structures in condensed chemical systems. Interesting patterns, relevant to chemistry, can be derived from those hyperbolic patterns met above. An understandable objection by the practising chemist is similar to that raised by our colloidal chemist, mentioned at the beginning of this article: Why complicate matters when atoms and molecules reside in 3D euclidean space? Our answer is this. In many respects, we simplify the 3D problem by working in 2D space, albeit curved. In particular, we have seen above that we can tune packing densities rather readily. Further, novel patterns, including ribbon tilings and forests are generated, whose analogues in 3D euclidean space, $\mathcal{E}^3$, turn out to be of some interest to chemistry.

Our recipe for moving from $\mathcal{H}^2$ to $\mathcal{E}^3$ is described in detail elsewhere.[5] Essentially, we choose hyperbolic surfaces in $\mathcal{E}^3$, that can be readily 'unwrapped' into $\mathcal{H}^2$. Our construction from $\mathcal{H}^2$ to $\mathcal{E}^3$ reverses this process: We map from $\mathcal{H}^2$ onto those surfaces, then embed the surfaces in $\mathcal{E}^3$. The technique allows us to move between $\mathcal{H}^2$ and $\mathcal{E}^3$, provided the symmetries of our pattern in $\mathcal{H}^2$ are commensurate with $\mathcal{E}^3$ (more accurately, with some surface embedded in $\mathcal{E}^3$). The modular group, underlying Fricke and Klein's image, has orbifold symmetry *23∞. The presence of *∞ symmetry is incompatible with allowed symmetries of $\mathcal{E}^3$, and patterns with this symmetry cannot be projected to $\mathcal{E}^3$ without some symmetry mutation. Many examples of hyperbolic orbifold symmetries that are commensurate with $\mathcal{E}^3$ are known, thanks to parametrization studies of infinite periodic minimal surfaces (IPMSs). The allowed in-surface (intrinsic 2D) symmetries of IPMSs are a good guide to admissible symmetries of $\mathcal{H}^2$ for mapping from $\mathcal{H}^2$ onto $\mathcal{E}^3$.

IPMSs are translationally periodic (with three lattice vectors), symmetric, saddle-shaped surfaces. Their geometries and topologies have been explored at length in the past twenty years, largely due to their relevance to chemical structures.[7] The intrinsic symmetries of IPMSs are well studied, as they determine the 3D euclidean form of the surface.[8] In order for the projection of $\mathcal{H}^2$ into $\mathcal{E}^3$ to give a translationally periodic pattern, the underlying pattern in $\mathcal{H}^2$ must be commensurate with the kaleidoscopic groups characteristic of the relevant IPMS (namely form a suitable subgroup of the surface group).

The mapping from $\mathcal{H}^2$ to $\mathcal{E}^3$ is a projection. Though the dimension of $\mathcal{H}^2$ is one less than $\mathcal{E}^3$, it is vastly more 'spacious' than $\mathcal{E}^3$. Indeed, $\mathcal{H}^2$ is, in many senses, closer to $\mathcal{E}^\infty$ than $\mathcal{E}^3$. For example, the area of discs in $\mathcal{H}^2$ grows exponentially with radius (Equation (*1*), while that of euclidean balls grows as r^n, which matches that of $\mathcal{H}^2$ only in the limit, $n \to \infty$. (That observation implies that we can project to higher dimensional euclidean spaces also.)

For brevity, we choose here the most symmetric kaleidoscopic group in $\mathcal{H}^2$ that is commensurate with $\mathcal{E}^3$, the simplest and best-known IPMSs, three cubic, genus-three IPMSs known as the P(rimitive), D(iamond), and G(yroid) surfaces. These surfaces all share a common in-surface hyperbolic symmetry group, *246, introduced above. That imposes the significant constraint that $\mathcal{H}^2$ patterns must be subgroups of *246 to be mapped to $\mathcal{E}^3$ via the P, D, or G IPMS. (We note that many other hyperbolic kaleidoscopic groups can be chosen also, depending on the choice of IPMS!). We have demonstrated above that different pattern *classes* derived from Fricke and Klein's image—disc packings, nets, trees, and decorated trees, can be transposed into symmetries commensurate with *246, giving disc packings, nets, and (decorated) forests. It is those derivative patterns, shown in Figures 10–14, that we discuss here, as they can be mapped to $\mathcal{E}^3$.

Table 1. Projections of 4-coordinated nets from $\mathcal{H}^2$ to $\mathcal{E}^3$, via the primitive, diamond, and gyroid surfaces

The nets are identified by their vertex symbols in $\mathcal{H}^2$ and $\mathcal{E}^3$ projections by their standard zeolite code (where applicable), plus space group and vertex positions

2D net	P surface	D surface	G surface
(6.6.6.6)	SOD $Im\bar{3}m$ Vertices at 12d [1/4, 0, 1/2]	NbO $Pn\bar{3}m$ (origin 1) vertices at 6d [0, 1/2, 1/2]	S* $Ia\bar{3}d$ vertices at 24d [3/8, 0, 1/4]
(6.4.6.4)	– $Im\bar{3}m$ Vertices at 24h [0, y, y] ($y = 0.3249$)	SOD $Pn\bar{3}m$ vertices at 12f [1/4, 0, 1/2]	ANA $Ia\bar{3}d$ vertices at 48g [1/8, x, 1/4 – x] ($x = 0.3375$)

Nets and Extended Framework Structures

Nets, containing finite-sided polygons, have been (and are being) explored extensively due to their relevance to chemistry, particularly solid-state chemistry.[9] The cataloguing of nets in $\mathcal{E}^3$ has long been of interest to solid-state chemists, though is only very recently advanced beyond empirical enumeration, thanks to advances in tiling theory.[10] Our approach complements that work.

Consider the simplest nets derived above, (6.6.6.6) and (6.4.6.4). They map onto the P, D, and G surfaces to give a variety of nets in $\mathcal{E}^3$ (Table 1). Many (though not all) of these projections form extended framework structures.[11] Most of these are well known to chemists: They include the tetrahedral (Si, Al) 'T-atom' nets in the sodalite, faujasite, and analcime (Figs 15*a* and 15*b*) frameworks (SOD, FAU, and ANA in the *Atlas of Zeolites*[12]).

Two of these nets, (6.4.6.4) on the P surface and (6.6.6.6) on the G surface, have not been reported as zeolite or related frameworks. Are they chemically interesting? Vertices of the former net can be decorated with squares, giving the RHO zeolite framework (Fig. 15*c*).[13] The latter net has no known analogue in extended chemical frameworks, although it has been described by O'Keeffe,[14] who named it S* (with vertices at positions of the S* lattice complex, Fig. 15*d*). Its vertices define the Si positions in grossular (a garnet, $Ca_3Al_2Si_3O_{12}$).[15] Two-coordinated vertices can be inserted on edges on S*, to form a vertex-coordinated tetrahedral arrangement (Fig. 15*e*). The tetrahedra are distorted, but slight displacements, corresponding to cooperative rotations

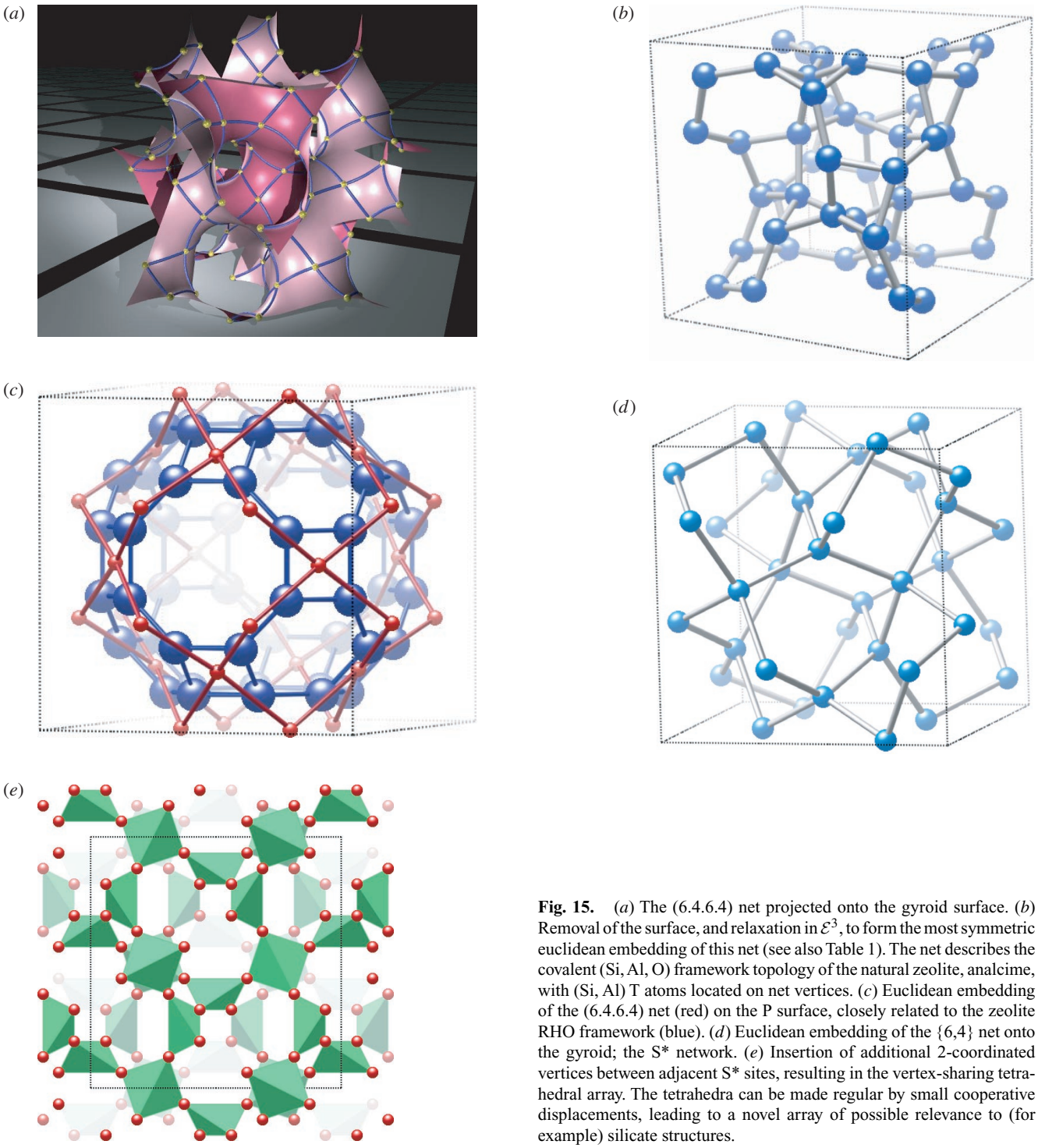

Fig. 15. (*a*) The (6.4.6.4) net projected onto the gyroid surface. (*b*) Removal of the surface, and relaxation in $\mathcal{E}^3$, to form the most symmetric euclidean embedding of this net (see also Table 1). The net describes the covalent (Si, Al, O) framework topology of the natural zeolite, analcime, with (Si, Al) T atoms located on net vertices. (*c*) Euclidean embedding of the (6.4.6.4) net (red) on the P surface, closely related to the zeolite RHO framework (blue). (*d*) Euclidean embedding of the {6,4} net onto the gyroid; the S* network. (*e*) Insertion of additional 2-coordinated vertices between adjacent S* sites, resulting in the vertex-sharing tetrahedral array. The tetrahedra can be made regular by small cooperative displacements, leading to a novel array of possible relevance to (for example) silicate structures.

of the edges in $\mathcal{H}^2$, render the tetrahedra regular in $\mathcal{E}^3$. This structure is a reasonable prima facie candidate for a dense silicate.

Two features emerge from the 2D hyperbolic perspective, that cannot be described in detail here. Firstly, the framework density, of relevance to designing large-pore frameworks, can be seen to scale with the ring size in $\mathcal{H}^2$. We thus conclude that low density (or rare) frameworks require *small* rings, a conclusion that appears at first counterintuitive in $\mathcal{E}^3$, yet agrees well with observed rare zeolite frameworks.[16] Indeed, quantitative lower bounds on framework densities for silicate and other frameworks can be deduced from this approach.[16] Secondly, the formation of *chiral* frameworks in $\mathcal{E}^3$ can be induced by the mapping process,[17] by choosing nets in $\mathcal{H}^2$ whose orbifolds are free of 2D reflections.

Dense Disc Packings

The disc packings in $\mathcal{H}^2$ of Figures 11 and 12 can also be projected to $\mathcal{E}^3$, giving sphere packings and associated structures. The projections are summarized in Table 2. The

Table 2. Projections of dense hyperbolic disc packings into $\mathcal{E}^3$, via the primitive, diamond, and gyroid surfaces

$\mathcal{H}^2$ pattern	Projection from $\mathcal{H}^2$ to $\mathcal{E}^3$ via		
2D disc packing	P surface	D surface	G surface
6-coordinated packing on *246 $\rho = 0.82843$ (Fig. 11)	Primitive cubic packing $Im\bar{3}m$ vertices at 8c [1/4, 1/4, 1/4]	Cubic close packing $Pn\bar{3}m$ (origin 1) vertices at 4b [1/4, 1/4, 1/4]	Body centred cubic sphere packing (6-coordinated) $Ia\bar{3}d$ vertices at 16a [0, 0, 0]
12-, 4-coordinated binary packing on *246 (A_2B_3) $\rho = 0.84385$ (Fig. 12b)	12-coordinated packing $Im\bar{3}m$ *6 vertices at 8c *4 vertices at 12d [1/4, 0, 1/2]	16-coordinated packing $Pn\bar{3}m$ (origin 1) *6 vertices at 4b *4 vertices at 6d [0, 1/2, 1/2] δ-Bi_2O_3 M_3P_2 (M = Mg, Cd, Zn) M'_3As_2 (M′ = Mg, Zn) Ag_2O_3	14-coordinated packing $Ia\bar{3}d$ *6 vertices at 16a *4 vertices at 24d [3/8, 0, 1/4] $Cd_{0.5}Bi_{1.5}O_{2.75}$ Al, Si sites in garnet

4z-coordinated disc packings of the *24($2z$) orbifolds map to very well-known packings in 3D euclidean space for the case $z = 3$ (Fig. 11)—the simple cubic, body-centred cubic (bcc), and cubic close-packed (ccp) arrays of spheres for the P, G, and D surfaces respectively. Note that the coordination number of the packings in $\mathcal{E}^3$ can increase beyond that in $\mathcal{H}^2$, due to extra spatial contacts.

The binary ($2z$,4)-coordinated A_2B_z pattern also leads to interesting structures in E^3. Again, consider the case $z = 3$ (A_2B_3). The D surface projection of that pattern (labelled here A_2B_3(D)) is a 'stuffed' ccp structure. The ccp array generates tetrahedral voids. The A_2B_3(D) packing gives a structure with only three-quarters of those tetrahedral sites occupied, with the *6 (A) sites mapped to those of a ccp lattice and the *4 (B) sites mapped to interstitials in $\mathcal{E}^3$ (Fig. 16*a*). (Filling *all* of these sites gives the fluorite structure type CaF_2.) The G surface projection (A_2B_3(G)) is a stuffed bcc array, with the *6 and *4 sites projected to bcc and interstitial locations in $\mathcal{E}^3$ respectively. Like the ccp lattice, we can describe the bcc lattice in terms of octahedra and tetrahedra, albeit irregular for the bcc case. The resulting structure consists of vertex-coordinated distorted octahedral, or distorted tetrahedral, arrays (Figs 16*b* and 16*c*). The interstitial B atoms occupy one-quarter of the distorted tetrahedral voids created by the bcc A-lattice.

A number of examples of the D and G packings have been discussed in the chemistry literature (see Table 2). The high temperature (δ) phase of Bi_2O_3 has been suggested to adopt an ordered arrangement of oxygen atoms in one modification,[18,19] although there remains some uncertainty in this model.[20] Partial replacement of Bi by Cd (with some sub-stoichiometry) forms the compound $Cd_{0.5}Bi_{1.5}O_{2.75}$. This has been reported to adopt the G structure (with fractional occupancy of the oxygen positions).[21] The common non-euclidean 2D arrangement of the D and G projections affords a useful structural link between these two materials. The D array is also relevant to the family of silver oxides. Though some uncertainty surrounds the precise nature of the material with stoichiometry Ag_2O_3, an early structural determination reports the $Pn\bar{3}m$ (D) structure.[22] The D array has also been reported for a number of phosphides and arsenides (Table 2).[23] (These early studies incorrectly reported the space group as $P4_232$, rather than $Pn\bar{3}m$. Later studies cast some doubt on the structure, and reassessment of these structures remains desirable.) Finally, the G packing is related to the structure of garnet, $Ca_3Al_2Si_3O_{12}$. The arrangement of Si and Al 'framework' atoms in this mineral is precisely that of the G packing![24]

Rare Disc Packings and Vertex Decorations

The issue of *low* density (rare) sphere packings in $\mathcal{E}^3$ is one of relevance to structures in crystals, notwithstanding the usual emphasis on dense packings. Examples of rare packings in $\mathcal{H}^2$ have been introduced, based on z-coordinated (decorated) trees.

The *decorated* $z = 3$ example (with density, $\rho = 0.19677$) is a natural 2D hyperbolic generalization of the rarest 2D euclidean disc packing, $\rho = 0.3907$ (Figs. 7*b* and 7*c*). This packing, with equivalent discs, can be mapped onto the G, D, *or* P surfaces, resulting in a (three-coordinated) 3D euclidean sphere packing, with cubic symmetry ($I4_132$). This packing—described already in 1933 by Heesch and Laves—is conjectured to be the rarest sphere packing with equivalent spheres.[25] An exhaustive catalogue of three-coordinated sphere packings by Koch and Fischer also identified this packing (labelled by them *3/3/c1*).[26] They established that among all three-coordinated sphere packings with equivalent spheres in E^3, *3/3/c1* is the rarest (with a filling factor of 0.0555, Fig. 17). Evidently, the construction of rare packings in $\mathcal{H}^2$ is a useful route to construction of rare examples in $\mathcal{E}^3$.

The vertex-decoration process used to form the rare disc packing in Figure 7*b* from that of Figure 7*a* can be generalized to arbitrary values of z via replacement of each z-coordinated vertex in the original tree by a polygon (z). A distinct decoration process, that retains the original connectivity (z), is the following, illustrated in Figure 18. Replace each z-coordinated vertex by the complete graph, K_z. (This consists of a net containing z vertices, each $(z-1)$-coordinated to all other vertices. In 2D, we can draw K_z as a star with z vertices.)

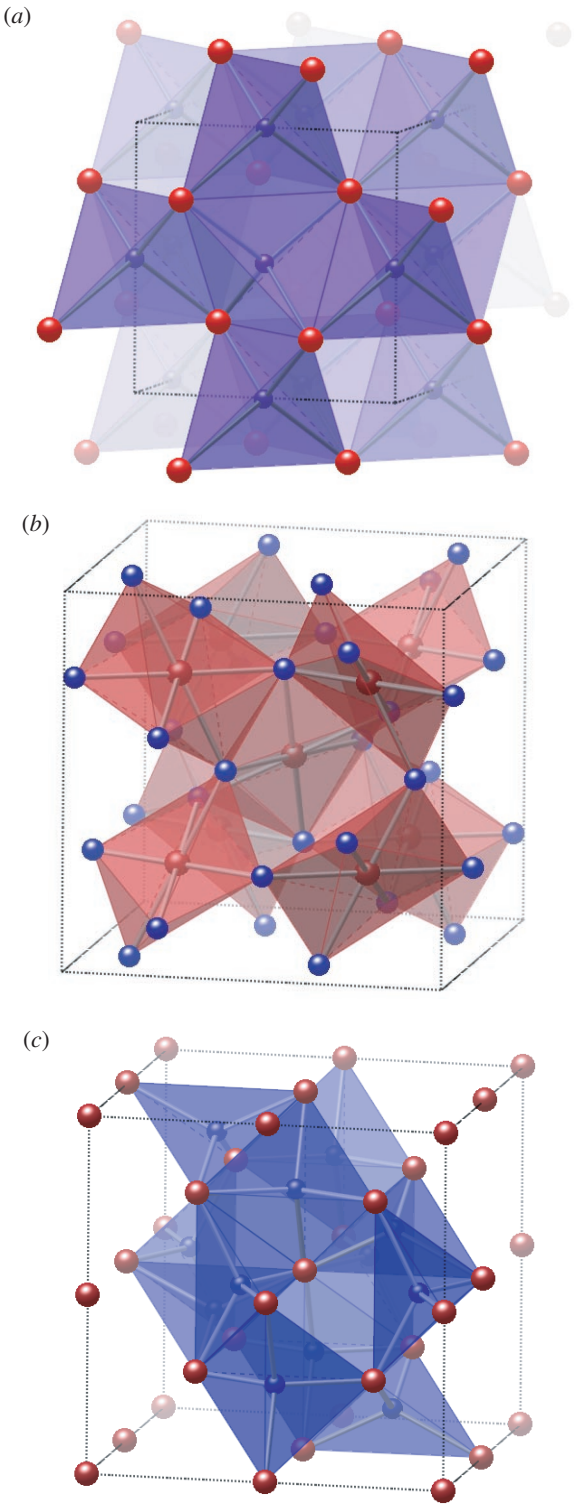

Fig. 16. Projections of the binary A_2B_3 disc packing (Fig. 14) via (*a*) the diamond and (*b*) the gyroid surfaces. The structures can be described in conventional terms as corner-coordinated (*a*) regular tetrahedra and (*b*) irregular octahedra or (*c*) irregular tetrahedra.

Now decorate all vertices of the z-coordinated tree by K_z, resulting in a new z-coordinated net. This 'star-decoration' process is identical to that invoked to generate the rare three-coordinated disc packing ($z = 3$), but yields distinct nets for larger z.

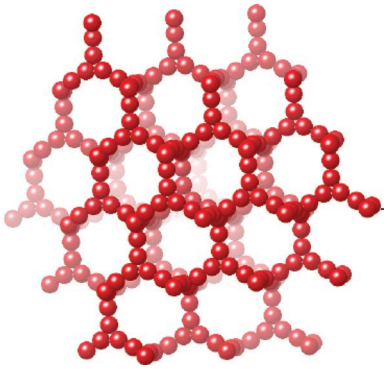

Fig. 17. View of the rarest (least dense) three-coordinated sphere packing in $\mathcal{E}^3$ with equivalent spheres; likely also to be the rarest (equivalent) sphere packing in $\mathcal{E}^3$.

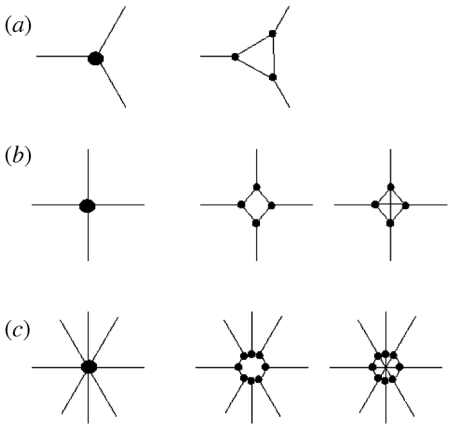

Fig. 18. Vertex decoration process for (*a*) 3-, (*b*) 4-, and (*c*) 8-coordinated nets. Vertex decoration by a z-gon results in 3-coordinated vertices (middle column). Replacement of the vertex by a complete graph of degree z (rightmost) maintains the original connectivity (z), giving a 'star-decorated' vertex. Real vertices are dotted (crossings due to the planar picture are not). Both processes are identical for $z = 3$. For higher connectivities, they are distinct.

In general this decoration process leads to edge crossings in $\mathcal{H}^2$ (or disc overlap in the related disc packing), but is realizable without overlap in 3D (or higher) space. When $z < 5$, we can relax the star in $\mathcal{E}^3$, generating z-coordinated rare nets. Some of these examples are already known to structural chemists. For example, decorations of the regular 3- and 4-coordinated trees by K_3 and K_4 respectively and projection onto the D surface, result in the nets *Y*3* (see Fig. 25*c*) and *D4*, known already to O'Keeffe.[9b] Like their hyperbolic counterparts, these euclidean 3D nets are also rare—although still rarer examples are known.[9b]

Trees, Forests, and Interpenetrating Nets

Recall that low density ('rare') disc packings are related to trees in $\mathcal{H}^2$ (Fig. 7). A series of z-coordinated disc packings result by centring discs of radius $l/2$ at vertices of regular trees, $T(l, z)$. As before, to map those low density structures into $\mathcal{E}^3$, we choose an orbifold symmetry of the tree that is commensurate with $\mathcal{E}^3$, such as *246. Recall that regular 3- and 4-coordinated trees can be packed densely in $\mathcal{H}^2$ with symmetries that are subgroups of *246 (Figs. 10*a* and

Table 3. Projections of three-coordinated trees in $\mathcal{H}^2$ to $\mathcal{E}^3$ via the primitive, diamond, hexagonal, and gyroid surfaces
The edge lengths in the H surface trees, l_1, and l_2, are variable, depending on the axial ratio of the surface

$\mathcal{H}^2$ pattern	Projection from $\mathcal{H}^2$ to $\mathcal{E}^3$ via			
Trees	P surface	D surface	H surface	G surface
T\{arcosh(3),3\} *2223		4 interpenetrating Y*+ (each net $I4_132$; $P4_232$ in toto)		2 interpenetrating Y*+ (each net $P4_132$; $I4_132$ in toto)
T\{arcosh(5),3\} 2*23	8 interpenetrating Y*+ (each net $I4_132$; $I432$ in toto)			
T\{arcosh(5),4\} *2224		2 interpenetrating diamond nets (each net $Fd\bar{3}m$; $Pn\bar{3}m$ in toto)		
$T(l_1,3)$ *2226			3 interpenetrating *(8,3)*-*c* nets (each net $P6_3/mmc$; $P6_3/mcm$ in toto)	
$T(l_2,3)$ *2226			3 interpenetrating graphite stacks (each stack $P2$; $P6$ in toto)	

10*b*). Specific members project to $\mathcal{E}^3$ (via P, D, or G surfaces) to form multiple interpenetrating three-dimensional extended frameworks.[27] Some examples found to date are tabulated in Table 3. The 3-coordinated examples result in interwoven Y^* nets, identified within a chemical context by Wells (his *(10,3)*-*a* net)[9a] and later O'Keeffe, who has pointed out that it is the *only* 3-coordinated net with symmetrically identical vertices and edges. The most symmetric (*2224) forest containing 4-coordinated trees projects onto the D surface to give a pair of interpenetrating diamond nets in $\mathcal{E}^3$.

Interest among chemists in interpenetrating nets has been substantial; with significant contributions by Australian chemists.[28,29] These nets define the bonding skeletons in coordination polymers, metallo-organic crystals of interest to the (somewhat euphemistically named) field of 'crystal engineering', perhaps better termed 'reticular synthesis'.[30] Coordination polymers are of interest to materials scientists, due to their magnetic, electronic, and porous features. Interpenetrating Y* and diamond nets are particularly common examples of these materials. Indeed, all the examples listed in Table 3—and many more—have been crystallized in the laboratory and earlier described by Wells.[9a]

Our projection technique leads also to novel topologies and geometries not yet described elsewhere in a chemical context, or synthesized. Two interesting examples, that exemplify the topological and geometrical complexity that can be realized by this technique are derived by projection of three-coordinated forests onto another IPMS, the (hexagonal) H surface. The first consists of three interpenetrating hexagonal *(8,3)*-*c* nets of Wells[9a] (Fig. 19). Each *(8,3)*-*c* net displays symmetry $P6_3/mmc$ ($a = (5/2)\sqrt{3}$ and $b = \sqrt{3}$ for unit net edges) with nodes at 2c (1/3, 2/3, 1/4) and 6h (x, $2x$, 1/4) ($x = 5/6$). The symmetry of the total pattern, containing three equivalent nets, is $P6_3/mcm$ ($a = 5/2$ and $b = \sqrt{3}$ for unit net edges) with nodes at 2a (0, 0, 1/4) and 6g (4/10, 0, 1/4). The second contains three interwoven stacks of graphite nets, arranged to form a 3D lattice (Fig. 20). The complete pattern has symmetry $P6$ ($a = 3$ and $c = \sqrt{3}$ for unit edges) and nodes at 6d (1/2, 1/6, 0) and 6d (1/2, 1/3, 1/2) (each graphite stack has symmetry $P2$). In both cases each component net can be realized with equal edge lengths and angles (Table 3). (The closest separation between nodes of different *(8,3)*-*c* nets is a factor of $(1/2)\sqrt{3}$ smaller than the edge length).

The Nature of Interpenetration: Links and Knotted Graphs

The concept of interpenetrating nets poses a number of challenges to the theorist. A fascinating question, posed already by chemists, is how to quantify notions of interpenetration.[31] Sophisticated mathematical signatures are required. In that context, it is interesting to compare the cases listed in Table 3 with the (topologically) complex examples of interpenetrating nets known to chemists, such as the multiple interpenetrating diamond nets.[32] One measure is the degree of interpenetration, recognized decades ago by Wells. An essential concept for analysis of interpenetration is that of 'strong rings'.[30]

Carlucci et al. have recently analyzed coordination polymeric entanglement networks in terms of *links* in $\mathcal{E}^3$.[31] Links are simpler than knots: They consist of interlocked, vertex-free rings. The simplest n-links, can be drawn as n loops on a (genus-one) torus, each with equivalent homotopy (winding number around the various channels) on the torus images (for example, Fig. 21*a*).

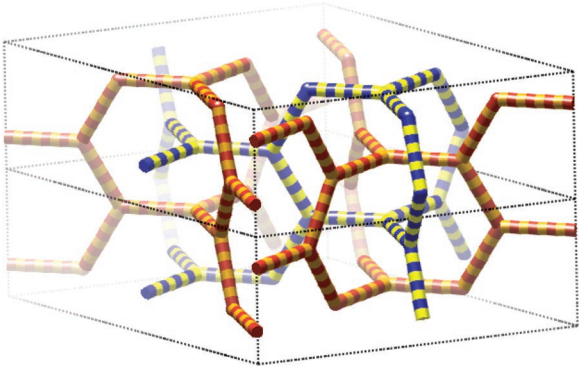

Fig. 19. A trio of (*8,3*)-*c* interpenetrating nets generated by projection of an irregular forest onto the H surface, with a single hexagonal unit cell marked by dashed edges. (One net is coloured differently for clarity.)

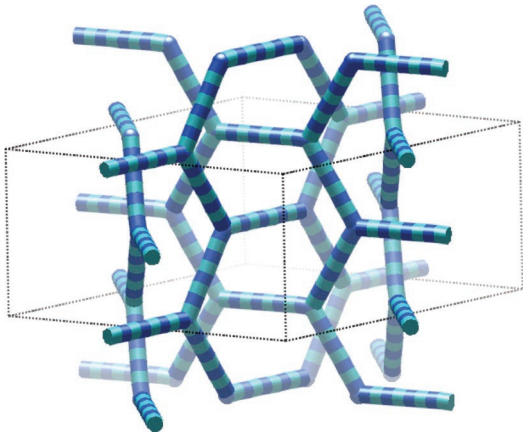

Fig. 20. A second example formed by projection of a (regular) 3-coordinated forest onto the H surface (with a hexagonal unit cell indicated by dashed edges).

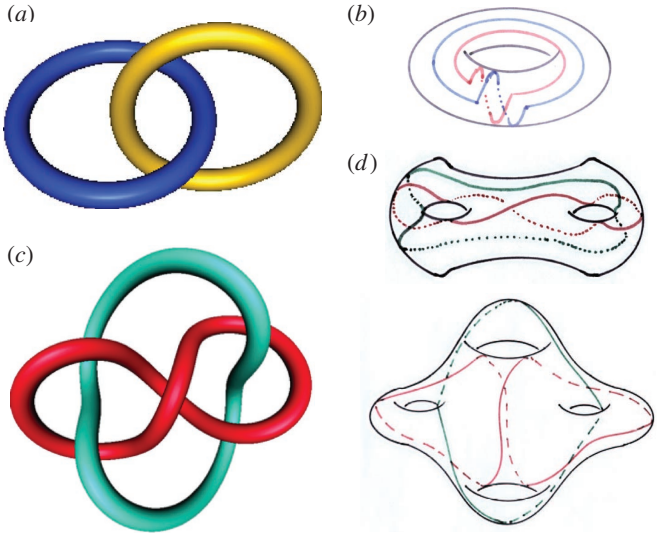

Fig. 21. Embeddings of simple links as closed, non-intersecting windings on hyperbolic surfaces. (*a*) The Hopf link. (*b*) The Hopf link on the genus-one torus. (*c*) The (5.2.1) link. (*d*) The (5.2.1) link embedded on (top) the genus-two torus and (bottom) the genus-four torus.

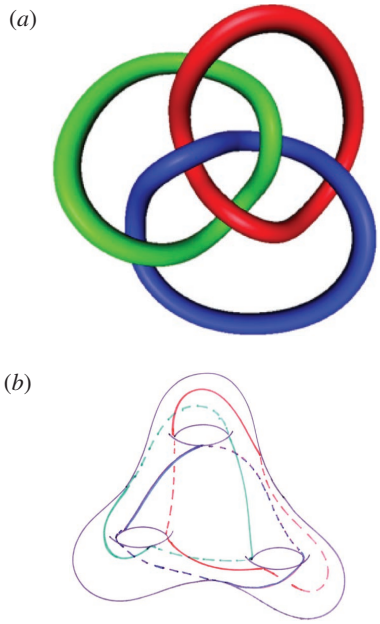

Fig. 22. (*a*) The three-component Borromean rings link. (*b*) Embedding of the Borromean ring link on the genus-three torus.

More complex links are decorations of multi-holed tori, with genera larger than one (for example Fig. 21*d*). We can see from these examples that the link character is encapsulated by the surface topology and homotopy class of each loop. How does this relate to our 2D approach? We can view links as decorations of surfaces with *lines*, just as our interpenetrating nets are surface decorations by (forests of) *trees*. Further, *any* link can be traced as a set of non-intersecting lines (one per link) on a surface, usually a multi-holed torus. Within $\mathcal{H}^2$, the pattern due to a link is a general *line* array or a forest of 2-coordinated trees. For example, the Borromean ring link can be embedded on a genus-three torus (see Fig. 22).

Further characterization of the network interpenetration is possible by the following construction. We take a unit cell of the IPMS and 'compactify' it, gluing surface points that are linked by a translation vector of the cell. This procedure is formally identical to periodic (Born–von Karman) boundary conditions; it results in a boundary-free surface, with donut-style handles joining elements that are identical under the translations induced by the unit cell. The compactification is also applied to the tree edges on the surface, resulting in a *knotted graph* of connectivity *z* (for a *z*-tree). The examples of interpenetrating nets we have generated so far (by projection of forests built of identical trees, Table 3) display a common interpenetration character. They consist of *n* components (each one a disjoint graph), with every strong ring of a particular component threaded by edges of *all* other components. For example, a pair of interpenetrating simple cubic nets (that define the channels of the P surface, Fig. 23*a*) can be compacted, to give a pair of interwoven 3-coordinated graphs (Fig. 23*b*). The resulting knotted graph (Fig. 23*c*) is a branched version of the simplest *link* with two components, the (2-coordinated) Hopf link.[32] This knotted graph reticulates the genus-three torus.

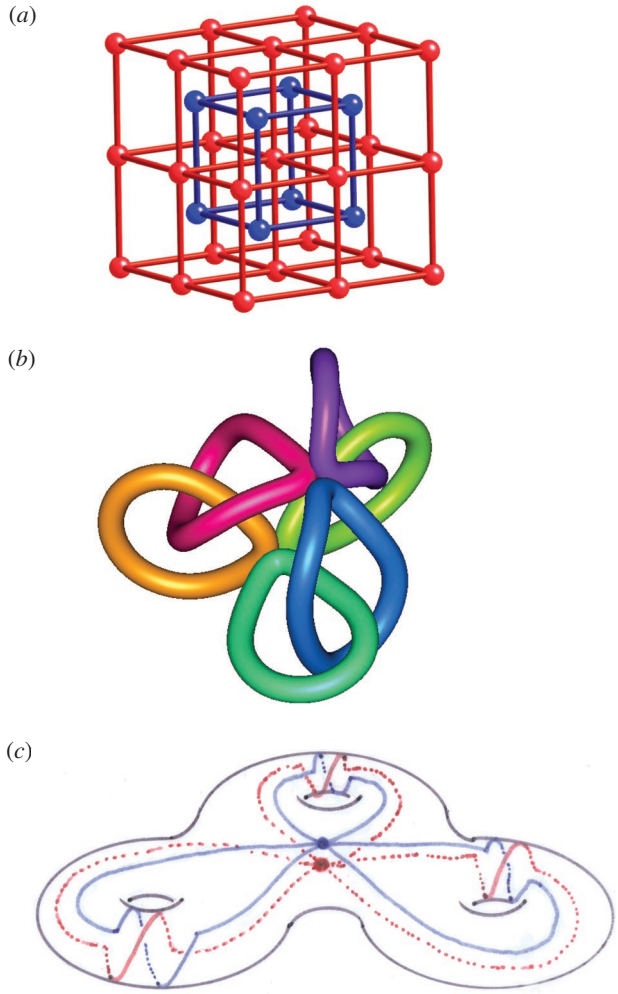

Fig. 23. (*a*) A pair of interpenetrating simple cubic nets (that define the channel structure of the P surface). (*c*) Mapping of the graph in (*a*) by gluing of graph elements separated by a lattice vector of the (conventional cubic bcc) unit cell, mapped onto the genus-three torus, that describes the topology of the glued P surface unit cell. (Note that the diagram conserves the topology of the P pattern, not its geometry.) (*b*) Knot image of the edges in (*b*) relaxed in $\mathcal{E}^3$. The resulting knotted graph contains two disconnected components, consisting of three loops sharing a vertex. Individual rings of each component graph are mutually threaded in the manner of the Hopf link.

The observation that interpenetration can be designed by projections of lines and trees from $\mathcal{H}^2$ into $\mathcal{E}^3$ has numerous ramifications. For example, a route to construction of multiple interpenetrating networks with a *deficiency* of interpenetration is suggested by the dual net to Fricke and Klein's pattern, and the decorated forests that emerge from that pattern (Fig. 14). The examples of Table 3 demonstrate that projection of trees allows for interpenetration. However, the presence of finite rings in the ribbon- and star-decorated trees—in addition to the unclosed infinite loops—implies the presence of some rings in the projected structures that are not interpenetrated. Indeed, as the number of finite rings decorating each tree vertex in the ribbon-decorated patterns in $\mathcal{H}^2$ increases, the degree of interpenetration decreases. Ribbon decorations of regular 3- and 4-coordinated trees packed into forests project in $\mathcal{E}^3$ to *partially* interpenetrating structures.

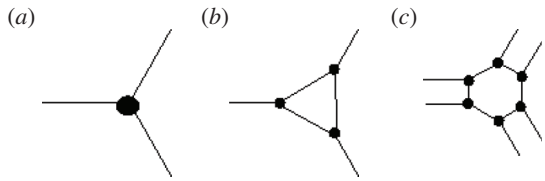

Fig. 24. (*a*) An undecorated vertex of a 3-coordinated tree and its decoration by (*b*) polygons and (*c*) ribbons respectively.

The degree of interpenetration is evident from the pattern in $\mathcal{H}^2$. Trees—with *no* finite rings in $\mathcal{H}^2$—result in threading of *all* rings in their $\mathcal{E}^3$ projections. Decorated trees, containing a fraction of vertices adjacent to rings, are partially threaded such that all rings visible in the $\mathcal{H}^2$ image remain unthreaded in $\mathcal{E}^3$. Consider, for example, the decorations of three-coordinated tree vertices shown in Figure 24. The polygonal decoration (Fig. 24*b*) results in a threading factor of 2/3 (one-third of the angles contains a ring), while the ribbon decoration (Fig. 24*c*) gives interpenetrating nets with a threading factor of 1/3 (as two-thirds of the angles are now contained within a ring). We can apply those decorations to all the interpenetrating examples of projected Y^* nets, listed in Table 3, forming interpenetrating structures with various threading factors.

Projections of single 3-coordinated trees and polygon-decorated and ribbon-decorated trees give to the chiral graphs Y^*+ (or Y^*-), Y^*3+ and Y^**(ribbon)*$+$, respectively. Multiple copies of a single enantiomer of each can be intergrown to give the cases listed in Table 3, with varying degrees of interpenetration. The graphs are illustrated below (Fig. 25).

These examples reveal some of the power of the approach. Concepts of knottedness, handedness, and interpenetration are readily controlled within $\mathcal{H}^2$. The observation that links and knotted graphs can be generated by non-intersecting patterns in $\mathcal{H}^2$ (and subsequent projection to $\mathcal{E}^3$) is an important one. Indeed, *we can generate nets of arbitrary topological complexity from the projection process*.

Novel Honeycombs and Sponges from Forests

We close with an example of relevance to colloid science. The foregoing discussion of interpenetrating nets can be used as a basis for generating novel surface partitions of space. These partitions, which define the bounding walls of immiscible microdomains within the materials, are generalizations of the more familiar surface forms of relevance to lyotropic and thermotropic liquid crystals and block copolymer melts.[7] These include hexagonal honeycombs and bicontinuous sponges, based on the geometry of the P, D, and G IPMSs. It is now evident that the repertoire of forms available for molecular self-assembly is far richer than previously imagined.

The surface partitions carve $\mathcal{E}^3$ into interwoven channel structures. Thus, formally, the familiar honeycomb structure, characteristic of hexagonal mesophases, consists of a hexagonal array of parallel rods, and the D surface separates a pair of interpenetrating diamond nets. We can derive new partitions for *any* interpenetrating array of rods or nets. Given the wealth of interpenetrating patterns now available, there is a corresponding wealth of novel surface structures.

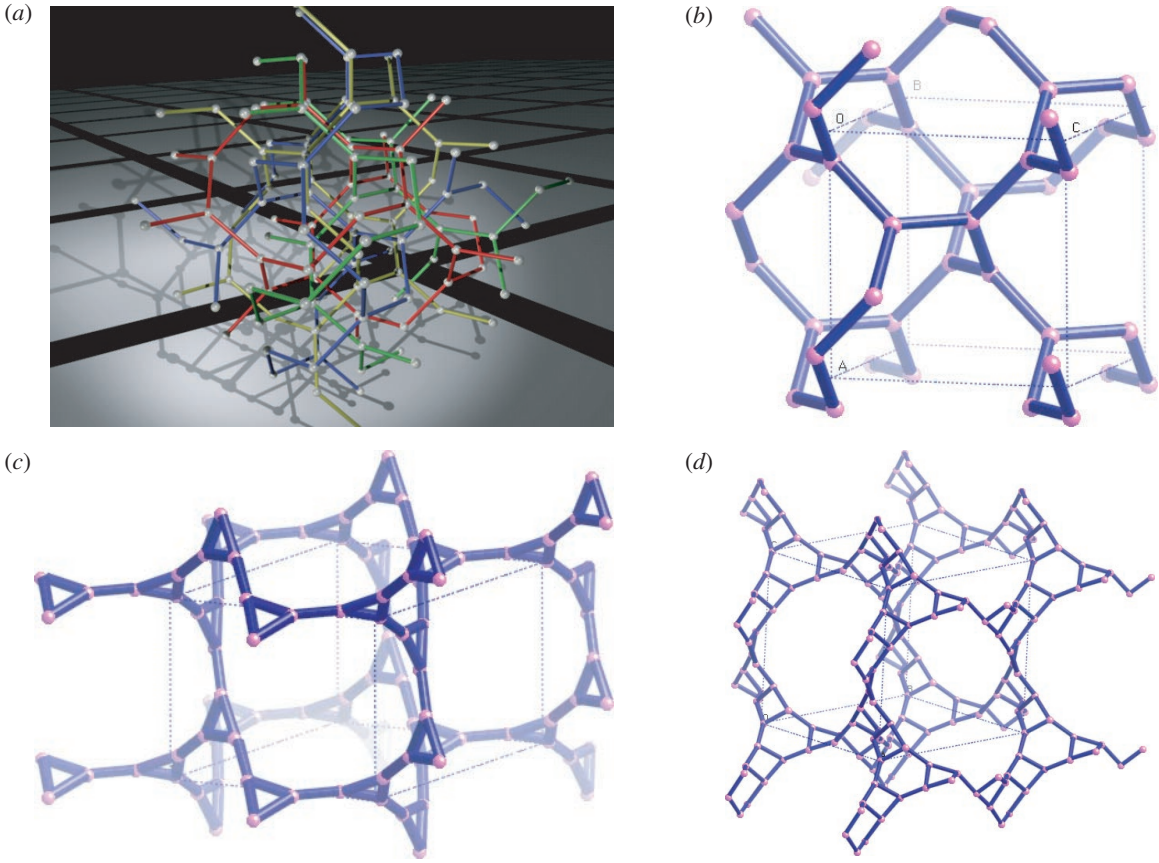

Fig. 25. (*a*) Projection of a hyperbolic forest of 3-coordinated trees (Fig. 10*a*) into $\mathcal{E}^3$ via the D surface, giving four identical interpenetrating enantiomeric *Y** graphs (compare Table 3). Examples of enantiomeric 3-coordinated graphs generated by projection of trees and decorated trees. (*b*) The cubic three-coordinated graph, *Y** (whose vertices form the lattice complex *Y***), (*c*) *Y*3*, and (*d*) *Y*(ribbon)*. Intergrowth of identical copies of these graphs (as in (*a*)) results in decreasing degrees of interpenetration from (*b*) to (*d*), due to the increasing number of rings per vertex induced by decoration processes shown in Figure 24.

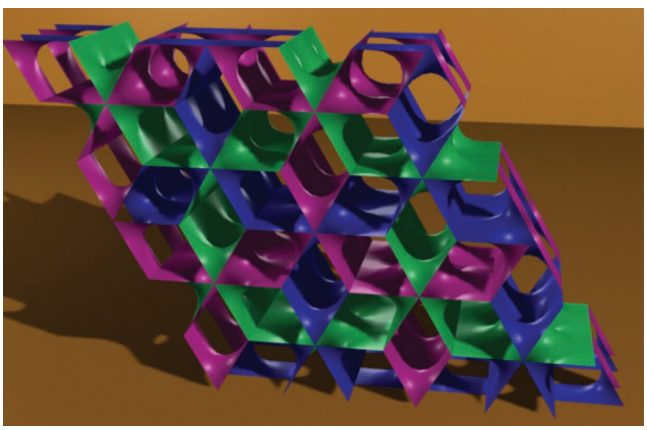

Fig. 26. The tricontinuous hexagonal minimal surface that trisects space into three equivalent labyrinths (shown in Figure 19).

The implications for molecular self-assembly have been discussed recently elsewhere.[33] Here we show just one example (Fig. 26). The tricontinuous hexagonal surface whose channel structure is that of Figure 19. This and related structures is likely to be as relevant to molecular assemblies as that of simpler IPMSs. Like IPMSs, these surfaces are characterized by relatively homogeneous, symmetric labyrinth structures.

Closing

It is clear from this multitude of examples that many of the subtleties of three-dimensional structure currently of interest to chemists are sometimes made visible within the hyperbolic perspective. Sphere packings, nets, polyhedral arrays, rod packings, interpenetrating nets, and complex surface partitions emerge from this construction. Evidently, there is a multiplicity of structural paradigms one can choose to model molecular and atomic crystalline arrangements, and there is no simple 'best' description. However, the flexibility of the hyperbolic approach does offer structural scientists a new way to design and describe complex patterns from a two-dimensional perspective. In some cases, that perspective offers a view of structural relationships invisible to a more conventional euclidean perspective.

The article has attempted to connect group theory, non-euclidean geometry, and condensed material structures. A possible response from chemists is the scepticism of colloid chemists, quoted in the Introduction, reflecting a current obsession with 'useful' science. A useful rejoinder to that obsession is that of Felix Klein himself, delivered in a lecture in the United States, from September 1892.

'*I am led to these remarks by the consciousness of a growing danger in the higher educational system of*

Germany—the danger of a separation between abstract mathematical science and its scientific and technical applications. Such separation could only be deplored; for it would necessarily be followed by shallowness on the side of the applied sciences, and by isolation on the part of pure mathematics.'[34]

Plus ça change!

Appendix: Schläfli Symbols and Orbifold Symmetry Notation

Schläfli symbols are commonly used to describe the *topology* of a net. We adopt the following conventions, suitable for 2D embeddings of a net. Suppose the net contains topologically equivalent vertices. Consider the 'vertex configuration' for a z-coordinated net at a specific vertex, which is common to the edges $e_1, e_2, \ldots, e_z$. We determine the polygonal size of all shortest ('strong') rings containing the vertex, and the z angles formed (in the 2D embedding) by adjacent edges e_j, e_{j+1}. Denote that polygon by n_j. The vertex configuration for the vertex in question is denoted by the symbol $(n_1.n_2 \ldots n_j \ldots n_z)$. For example, the hexagonal graphite ('chicken wire') net, or the network of mortar lines in a brick wall has vertex configuration (6.6.6) for all vertices. In cases where all rings are identical ($n_1 = n_2 = \cdots = n_j = \cdots = n_z$), we replace the vertex symbol by a Schläfli symbol (n,z) (or (6,3) for the previous example). In this paper we also include a crude symmetry descriptor in this topological measure, enclosing the symbol between braces $\{n,z\}$ in the cases where the net is *regular*, with symmetrically identical vertices, edges, and angles between adjacent edges. Thus, the graphite net is $\{6,3\}$ while the brick interstices are (6,3).

A more refined encoding of 2D (in-surface) symmetries is afforded by Conway's orbifold symbols. The symbol describes symmetry operators within a single fundamental domain of the symmetry group of the decorated surface. For the purposes of this article, we consider only two symmetry operators. These are 'cone points' and 'mirror strings'. Cone points are located at intersection of the axis of rotational symmetry (perpendicular to the surface) with the surface. We denote a cone point by the single digit a, with a-fold rotational symmetry. Mirror strings consist of contiguous paths of mirror lines (namely lines of reflection symmetry within the surface), with vertices on intersections of mirror lines (if they occur), located at cone points. These are denoted by the prefix * (mirror) followed by a digit string $bcd\ldots$ that describes the cone points at the intersecting mirrors in cyclic order around the mirror string. For example, the graphite net has cone points of orders 6, 3, and 2, all located at intersections of mirror lines. Its orbifold symbol is *632 (more familiar to crystallographers as the planar group *p*6*mm*). Generic orbifolds combine cone points and mirror strings. In those cases, cone points are listed first, followed by mirror strings. Thus, the brick pattern has orbifold symmetry 2*22 (*c*2*mm*).

Why bother with yet another notation system? The attraction of Conway's system is that it combines seamlessly symmetries for all three 2D geometries (euclidean, elliptic, and hyperbolic). No other simple notation system has been developed for groups in $\mathcal{H}^2$. Further, the symbols allow direct computation of the geometry class of the group and (where applicable) its index relative to sub- or super-groups. (The system also gives a trivial route to enumeration of all the plane and point groups!) Elliptic groups are better known to crystallographers as point groups. Orbifold notation thus allows a common notation for plane and point groups for crystallography. (For example, 4/*mmm* has orbifold symbol *224). While we do not expect crystallographers to adopt the notation in a hurry, we find it less ad hoc and more friendly than the conventional, inconsistent symbols used by spectroscopists and crystallographers.

Acknowledgments

We thank Prof. Michael O'Keeffe (Arizona State University) for inspiration and concrete assistance. We are also grateful to Dr Christophe Oguey (Cergy Pontoise University) for his contributions to this work. The figures of knots and links were generated with the *KnotPlot* package, freely available[35] thanks to the efforts of its creator, Dr Rob Scharein.

References

[1] F. Klein, R. Fricke, *Vorlesungen der Theorie der elliptischem Modulfunktionen*, *Bd. 1* [reprint **1966** (Johnson: New York, NY; Teubner: Stuttgart)]. We hasten to point out that we came to this reference circuitously. Klein's image was first encountered in a brilliantly accessible recent book: D. Mumford, C. Series, D. Wright, *Indra's Pearls. The Vision of Felix Klein* **2002** (Cambridge University Press: Cambridge).

[2] J. H. Conway, in *Groups, Combinatorics and Geometry—London Mathematical Society Lecture Note Series* **1992** (Cambridge University Press: Cambridge). See also: J. H. Conway, D. H. Huson, *Struct. Chem.* **2002**, *13*, 247.

[3] See: D. Wells, *The Penguin Dictionary of Curious and Interesting Geometry* **1991** (Penguir: London); originally from H. Meschkowski, *Unsolved and Unsolvable Problems in Geometry* **1966** (Oliver & Boyd: London).

[4] B. Söderberg, *Phys. Rev. E* **1993**, *47*, 4582.

[5] S. T. Hyde, C. Oguey, *Eur. Phys. J. B* **2000**, *16*, 613.

[6] The notion of 'greater' or 'lesser' symmetry refers to the area of the fundamental domain, which scales with the absolute magnitude of the orbifold characteristic (or 'cost'), computed readily from the Conway orbifold symbol (ref. [2]).

[7] S. T. Hyde, S. Andersson, K. Larsson, Z. Blum, T. Landh, S. Lindin, B. W. Ninham, *The Language of Shape* **1997** (Elsevier: Amsterdam).

[8] A. Fogden, S. T. Hyde, *Acta Cryst. A* **1992**, *48*, 575.

[9] See, for examples: (*a*) A. F. Wells, *Three-Dimensional Nets and Polyhedra* **1977** (John Wiley: New York, NY). (*b*) M. O'Keeffe, B. G. Hyde, *Crystal Structures. I. Patterns and Symmetry* **1996** (Mineralogical Society of America: Washington, DC). (*c*) M. O'Keeffe, M. Eddaoudi, H. Li, T. Reineke, O. M. Yaghi, *J. Solid State Chem.* **2000**, *152*, 3.

[10] O. Delgado Friedrichs, A. W. M. Dress, D. H. Huson, J. Klinowski, A. L. Mackay, *Nature* **1999**, *400*, 644.

[11] This identification was the initial impetus to the study of IPMSs and their relation to crystal structures; see ref. [8]. The projection technique describe here is a later development (ref. [5]).

[12] C. Baerlocher, W. M. Meier, D. H. Olson, *Atlas of Zeolite Structure Types* **2001** (Elsevier: Amsterdam); www.iza-structure.org/databases/.
[13] M. Eddaoudi, J. Kim, D. Vodak, A. Sudik, J. Wachter, M. O'Keeffe, O. Yaghi, *Proc. Natl. Acad. Sci. U. S. A.* **2002**, *99*, 4900.
[14] M. O'Keeffe, *Z. Kristallogr.* **1991**, *196*, 21.
[15] O. Delgado Friedrichs, J. Plévert, M. O'Keeffe, *Acta Cryst. A* **2002**, *58*, 77.
[16] S. T. Hyde, *Acta Cryst. A* **1994**, *50*, 753.
[17] S. T. Hyde, S. Ramsden, in *Chemical Topology. Applications and Techniques* (Eds. D. Bonchev, D. Rouvray) **2000** (Gordon and Breach: Sydney).
[18] L. G. Sillen, *Arkiv Kemi Mineral. Geol.* **1938**, *12*, 1.
[19] A. A. Zav'yalova, R. M. Ivanov *Zh. Struk. Khim.* **1972**, *13*, 869.
[20] V. P. Zhukov, V. M. Zhukovskii, V. M. Zainullina, N. I. Medvedeva, *J. Struct. Chem.* **1999**, *40*, 831.
[21] L. G. Sillen, B. Sillen, *Z. Phys. Chem. B* **1941**, *49*, 27.
[22] B. Stehlik, P. Weidenthaler et al., *Coll. Czech. Chem. Commun.* **1959**, *24*, 1581.
[23] (*a*) L. Passerini, *Gazz. Chim. Ital.* **1928**, *58*, 655. (*b*) G. Natta, L. Passerini, *Gazz. Chim. Ital.* **1928**, *58*, 541.
[24] (*a*) H. Bartl, *Neues Jahrb. Mineral. Monatsh.* **1969**, 404. (*b*) G. A. Lager, T. Armbruster, J. Faber, *Am. Mineral.* **1987**, *72*, 756.
[25] H. Heesch, F. Laves, *Z. Kristallogr.* **1933**, *85*, 443.
[26] E. Koch, W. Fischer, *Z. Kristallogr.* **1995**, *210*, 407.
[27] S. T. Hyde, S. Ramsden, *Europhys. Lett.* **2000**, *50*, 135.
[28] S. R. Batten, R. Robson, *Angew. Chem. Int. Ed.* **1998**, *110*, 1558.
[29] C. J. Kepert, T. J. Prior, M. J. Rosseinsky, *J. Am. Chem. Soc.* **2000**, *122*, 5158.
[30] O. M. Yaghi, M. O'Keeffe, N. W. Ockwig, H. K. Chae, M. Eddaoudi, J. Kim, *Nature* **2003**, *423*, 705.
[31] (*a*) S. R. Batten, *CrystEngComm* **2001**, *18*, 1. (*b*) L. Carlucci, G. Ciani, D. M. Proserpio, *CrystEngComm* **2003**, *5*, 269.
[32] L. Carlucci, G. Ciani, D. M. Proserpio, S. Rizzato, *Chem. Eur. J.* **2002**, *8*, 1520.
[33] S. T. Hyde, G. E. Schroeder, *Curr. Opin. Coll. Interf. Sci.* **2003**, *8*, 5.
[34] F. Klein, *Gesammelte Mathematische Abhandlungen,* vol. 2, p. 231 [reprint **1973** (Springer: Heidelberg)].
[35] www.cs.ubc.ca/nest/Imager/contributions/scharein/KnotPlot.html.